TAMPEREEN TEKNILLINEN YLIOPISTO
TAMPERE UNIVERSITY OF TECHNOLOGY

Carolina Moilanen

Image Based Analysis and Modelling of Norway Spruce Compression

Julkaisu 1505 • Publication 1505

Tampere 2017

Tampereen teknillinen yliopisto. Julkaisu 1505
Tampere University of Technology. Publication 1505

Carolina Moilanen

Image Based Analysis and Modelling of Norway Spruce Compression

Thesis for the degree of Doctor of Science in Technology to be presented with due permission for public examination and criticism in Sähkötalo Building, Auditorium S4, at Tampere University of Technology, on the 15 of November 2017, at 12 noon.

Tampereen teknillinen yliopisto - Tampere University of Technology
Tampere 2017

Doctoral candidate: Carolina Moilanen
Mechanical Engineering and Industrial Systems
Faculty of Engineering Sciences
Tampere University of Technology
Finland

Supervisor: Pentti Saarenrinne, Professor
Mechanical Engineering and Industrial Systems
Faculty of Engineering Sciences
Tampere University of Technology
Finland

Instructor: Tomas Björkqvist, Doctor
Automation and Hydraulic Engineering
Faculty of Engineering Sciences
Tampere University of Technology
Finland

Pre-examiners: Sven Bossuyt, Associate Professor
Department of Mechanical Engineering
Aalto University
Finland

Karl Murton, Doctor
Research Leader, Pulp, Paper & Pilot Plant Facilities
Scion
New Zeeland

Opponents: Lennart Salmén, Principal Scientist
Biorefinery and energy, RISE Bioeconomics
Adjunct Professor, Department of Chemical Engineering
Mid-Sweden University
Sweden

Sven Bossuyt, Associate Professor
Department of Mechanical Engineering
Aalto University
Finland

ISBN 978-952-15-4032-5 (printed)
ISBN 978-952-15-4041-7 (PDF)
ISSN 1459-2045

Abstract

The purpose of mechanical pulping is to separate fibres from the wood matrix and develop them into a form suitable for paper and board production. This fibre separation and development requires a large energy input, where much of this energy is dissipated into heat. Therefore, energy can be saved by designing a process with as little heat dissipation as possible. Numerical simulations would be an effective tool for solving such process design problems, but there is currently no suitable model for the behaviour of the wood.

To enable rational wood compression modelling, an image-based stress and strain analysis method for the split-Hopkinson pressure bar compression tests was developed. The results of this image-based stress analysis differed by only approximately 5 % from the strain gauge-based method. The image-based stress analysis is applicable to all split-Hopkins pressure bar testing. An image-based local strain measurement method was developed for earlywood and latewood analysis. The strain analysis method can also be used for strain analysis of other layered materials during high or low strain rate compression.

In this study, two models have been developed for the radial compression of Norway spruce: a simple compression model and a dynamic (strain rate dependent) compression model. Both models are based on high strain rate and quasi-static compression tests of Norway spruce at three different temperatures: room temperature, 100°C and 135°C. Native wood, chemically treated wood and mechanically fatigued wood were tested.

The local compression behaviour is important for mechanical pulping. The compression models developed here have separate layers for earlywood and latewood compression. The dynamic wood compression model can be used for numerical simulations of the wood deformations, which occur during mechanical pulping. These models are the first high strain rate and high temperature compression models for moist wood which have separate layers for earlywood and latewood. Initial quasi-static simulations were also conducted.

One important practical implication for mechanical pulping is that identically repeated compressions does not develop the wood fibres. The fibre should preferably be slightly rotated between compressions in order to get flexible in all directions. The significant difference in EW and LW stiffness suggests that the fibres need different kind of treatment. The wood also needs to be treated at the right temperature since the stiffness is strongly dependent on temperature.

Preface

First of all, I want to thank my supervisor, Professor Pentti Saarenrinne, for guiding me through this process; you have taught me a lot. I would also like to thank Dr. Tomas Björkqvist for all the support, comments on the manuscripts for publications and the help with the measurements. I could not have done this without you. Many of my colleagues have been jealous of the amount of support and guidance I have received from both of you. I would also like to thank Dr. Markus Honkanen for teaching me how the equipment works and helping me get started with both measurements and analysis. During this process, I have also found true friends in my colleagues. Thank you for making work fun!

The research for this thesis has been funded by the Academy of Finland, through the WoodMat project (140462). I am also grateful to the Doctoral Program of Concurrent mechanical Engineering for the funding and support. The Doctoral program provided good advice in the form of Professor Erno Keskinen and Professor Michel Cotsaftis.

I would like to thank Dr. Birgitta Engberg at Mid Sweden University for her support and good advice. I especially appreciate the co-operation with the split-Hopkinson measurements. I would also like to acknowledge Max Lundström and Staffan Nyström in the Mid Sweden University Material's lab for their help with the measurements. I would also like to thank Professor Mikko Alava, Dr. Juha Koivisto, Markus Ovaska and Dr. Amandine Miksic at Aalto University for their assistance with the quasi-static measurements.

The help of Dr. Lauri Salminen at VTT (currently at Andriz) has been invaluable. Lauri was in charge of our wood samples, participated in part of the measurements at Mid Sweden University and elaborately commented on the manuscripts for the publications.

My family and especially my three men at home, Pasi, Alexander and Onni have also taken part in this work. Pasi has not only believed in me, but also taken time to comment on my manuscripts. Alexander and Onni have in their own way made sure that mummy gets her mind off work. I love you and cannot thank you enough for your support.

Tampere 12.10.2017

Carolina Moilanen

Contents

Abstract i

Preface ii

Contents iii

List of Figures vi

List of Tables vii

Symbols and abbreviations viii

List of original publications ix

Author’s contribution x

1 INTRODUCTION 1

1.1 Background 1

1.2 Objectives and Scope 2

1.3 Outline and contribution 3

2 FULL-FIELD STRAIN MEASUREMENT 5

2.1 Digital image correlation 5

2.2 Speckle interferometry 6

2.3 From displacement to strain 6

2.4 Full-field strain measurement of wood 6

3 THE SPLIT-HOPKINSON PRESSURE BAR 9

3.1 The compression test technique 9

3.1.1 Stress and strain analysis 10

3.1.2 Image based stress analysis 10

3.2 Full-field split-Hopkinson measurement 11
3.3 Split-Hopkinson wood research 12
4 WOOD PROPERTIES 13
4.1 Wood compression behaviour 14
4.1.1 The impact of temperature on wood compression 15
4.1.2 The impact of strain rate on wood compression 15
4.2 Earlywood and latewood 15
4.3 Wood fatigue 16
5 WOOD MODELLING 19
5.1 Micromechanical models 19
5.2 Continuum models 21
6 MATERIALS AND METHODS 23
6.1 Material testing 23
6.1.1 Quasi-static material testing 24
6.1.2 High strain rate material testing 25
6.1.3 Measurement plan 26
6.2 Image-based strain analysis 27
6.2.1 Earlywood and latewood strain 28
6.3 Wood modelling 28
6.3.1 Static and dynamic model 28
6.3.2 Modelling of fatigue behaviour 29
7 RESULTS 31
7.1 Compression mechanisms 31

7.2 Stress strain curves 35
7.3 Wood compression model 36
7.4 Dynamic compression model 38
8 DISCUSSION 43
8.1 Uncertainty 44
8.2 Conclusions 46
8.3 Implications for mechanical pulping 47
8.4 Future work 48
REFERENCES 49

List of Figures

FIGURE 1 A schematic sketch of the SHPB set-up for compression tests. 10

FIGURE 2 Image based stress pulses according to Eq. 1 (red) and Eq. 3 (blue) compared to strain gauge measurement (black)..... 11

FIGURE 3 Images showing the orthogonal directions of wood **a)** for a spruce sample, **b)** an annual ring magnification image and **c)** the wood cell wall layers. 14

FIGURE 4 Diagram showing the most important steps of the wood sample preparation. 23

FIGURE 5 Images of a) the setup for the quasi-static measurements with the water bath b) a close-up of the sample in the testing machine and c) a schematic sketch showing the working principle of the testing machine. 24

FIGURE 6 Images of a) the encapsulated SHPB and b) the sample sandwiched between the SHPB bars..... 25

FIGURE 7 A flow diagram showing the quasi-static and high strain rate measurement temperatures and samples..... 26

FIGURE 8 Measured EW stress strain curves of native (blue) and fatigued (red) wood and the alternative modelling approaches: native model (black solid line), fatigued with reduced Ee (black dashed line) and fatigued with additional term (grey dashed line). 29

FIGURE 9 The high strain rate room temperature a) EW stress strain curves for the compression of native (blue) and fatigued (red) wood and images of native wood captured b) before compression, c) at the yield limit and d) in the end of the compression. 32

FIGURE 10 Images of fatigued wood during high strain rate compression at room temperature captured a) before compression, b) at the end of the elastic compression c) at the yield limit and d) at maximum compression. 33

FIGURE 11 EW strain as a function of time for one annual ring of a sample (blue) average of all annual rings of a sample (red) and one annual ring from fibre magnification measurement (black)..... 34

FIGURE 12 The quasi-static cyclic compression a) EW stress strain curve and images from b) the first pass and c) the second pass of the marked position. 34

FIGURE 13 High strain rate EW stress strain curves for native wood (blue), mechanically pre-fatigued wood (red) and chemically treated wood (pH 4 gray and pH 9 black) tested at a) 20°C, b) 100°C and c) 135°C. 35

FIGURE 14 High strain rate LW stress strain curves for native (blue), mechanically (red) and chemically (pH 4 gray and pH 9 black) treated wood tested at a) 20°C, b) 100°C and c) 135°C. 36

FIGURE 15 Measurement data and compression model for native (blue **x** and solid line) and fatigued (red **o** and dashed line) EW from high strain rate tests at a) 20°C, b) 100°C and c) 135°C….. 37

FIGURE 16 Measurement data and compression model for native (blue **x** and solid line) and fatigued (red **o** and dashed line) LW from high strain rate tests at a) 20°C, b) 100°C and c) 135°C……..... 37

FIGURE 17 Dynamic EW material model (red, blue, green and grey solid line) and high strain rate experimental data (red **x**, blue **x**, green **x** and grey **x**) and without the term $\varepsilon\eta$ (black dashed line) for a) native EW at 20°C, b) fatigued EW at 20°C, c) native EW at 100°C, and d) fatigued EW at 100°C. 39

FIGURE 18 Dynamic LW material model (red, blue, green and grey solid line) and high strain rate experimental data (red **x**, blue **x**, green **x** and grey **x**) and without the term $\varepsilon\eta$ (black dashed line) for a) native LW at 20°C, b) fatigued LW at 20°C, c) native LW at 100°C and d) fatigued LW at 100°C.…..... 40

FIGURE 19 Strain distributions from a) simulation and b) quasi-static compression test. 41

List of Tables

TABLE 1 High strain rate compression model parameters for native and fatigued wood at 20°C, 100°C and 135°C. 38

TABLE 2 Dynamic compression model parameters for native and fatigued wood at 20°C and 100°C. 40

TABLE 3 Comparison of conditions in mechanical pulping to experimental work and model prediction range..... 45

TABLE 4 The confidence intervals for the dynamic compression model material parameters..... 46

Symbols and abbreviations

Symbols

ε	Strain
$\dot{\varepsilon}$	Strain rate
ε_d	Densification limit
ε_{RR}	Strain in the radial direction
ε_{RT}	Shear strain in the radial-tangential plane
ε_{TT}	Strain in the tangential direction
ε_y	Yield limit
η	Dynamic parameter
σ	Stress
ρ	Density
A	Area
c	Wave propagation velocity
E_e	Young's modulus (elastic modulus)
E_d	Densification modulus
E_p	Plateau modulus (plastic modulus)
L	Longitudinal direction of wood
M	Middle lamella
P	Primary wall
R	Radial direction of wood
S1	Outer layer of secondary wall
S2	Middle layer of secondary wall
S3	Inner layer of secondary wall
t	Time
T	Tangential direction of wood
u	Displacement in the x direction or radial direction for wood
v	Displacement in the y direction or tangential direction for wood

Abbreviations

2D	Two-dimensional
3D	Three-dimensional
EW	Earlywood
DIC	Digital image correlation
ESPI	Electronic speckle pattern interferometry
FEM	Finite element method
LW	Latewood
MC	Moisture content
PIV	Particle image velocimetry
SHPB	Split-Hopkinson pressure bar
SI	Speckle interferometry

List of original publications

This thesis is based on the following publications, referred to as Publication I-V.

I. C. Moilanen, P. Saarenrinne, B.A. Engberg, T. Björkqvist (*2015)* **Image based stress and strain measurement of wood in the split-Hopkinson pressure bar**, *Meas.Sci.Technol.* 26, pp. 085206 (DOI 10.1088/0957-0233/26/8/085206) [JuFo 2]

II. C. Moilanen, B.A. Engberg, T. Björkqvist, L.I. Salminen, P. Saarenrinne (2014) **Local compression behaviour of pre-fatigued and chemically treated wood at high strain rate and high temperature**, *Proceedings of the International Mechanical Pulping conference,* Helsinki Finland June 2nd-5th 2014 [JuFo 1]

III. C. Moilanen, T. Björkqvist, B.A. Engberg, L.I. Salminen, P. Saarenrinne (2016) **High strain rate radial compression of Norway spruce earlywood and latewood**, *Cellulose* 23, pp.873-889. *[JuFo2]*

IV. C. Moilanen, T. Björkqvist, M. Ovaska, J. Koivisto, A. Miksic, B.A. Engberg, L.I. Salminen, P. Saarenrinne, M. Alava (*2017)* **Influence of strain rate, temperature and fatigue on the radial compression behaviour of Norway spruce**, *Holzforschung 71(6), pp. 505-514 [JuFo 1]*

V. C. Moilanen, T. Björkqvist, M. Ovaska, J. Koivisto, A. Miksic, B.A. Engberg, L.I. Salminen, P. Saarenrinne, M. Alava (2016) **Modelling and simulation of radial spruce compression to optimize energy efficiency in mechanical pulping**, *Proceedings of the International Mechanical Pulping Conference,* Jacksonville FL, September 26th-28th 2016, pp. 18-35 [JuFo 1]

Author’s contribution

The author has planned the experiments with the co-authors. The author has developed and implemented an image-based analysis and material modelling method.

I. The author developed the image-based analysis method with help from the co-authors. The author implemented the image-based analysis. The author also prepared the manuscript.

II. The author planned the measurements with the co-authors, the author was responsible for the image-based measurement and analysis. The author prepared the manuscript.

III. The author planned the measurements with the co-authors. The author was responsible for the image-based analysis. The author fitted the material parameters to the measurement data. The author also prepared the manuscript.

IV. The author planed the measurements with the co-authors. The author was responsible for the image based measurement and analysis. The author estimated the material parameters by fitting the model to the measurement data. The author prepared the manuscript.

V. The author planned the measurement with the co-authors and was responsible for the image-based measurement and analysis. The author estimated the material parameters for the material model and implemented the material model in the simulation software. The manuscript was prepared by Dr. Tomas Björkqvist during the maternity leave of the author. The author commented on the manuscript and prepared Figures 4-20.

1 Introduction

1.1 Background

The experimental work and the wood modelling presented in this thesis are aimed at optimizing the mechanical pulping process. In mechanical pulping, wood chips are broken into smaller fragments by repeated, high strain rate shear and compression loadings. There are two industrial-scale techniques which are used for this. The first technique involves pressing the wood logs against a revolving grindstone, while the second consists of disintegrating the wood chips in a disc refiner. The process both separates and softens the wood fibres into a form that is suitable for paper and board production. The processing conditions are hot, wet, and demand high strain rate loadings. Both the temperature and the strain rate have a significant effect on the stiffness of the wood, but testing the behaviour of moist wood under high temperatures and strain rates is a challenging task.

The defibration and fibre development in mechanical pulping process requires high energy input. This high energy consumption can be reduced by altering either the process, or the raw material itself. It has been shown that mechanical pre-treatment of the raw material can be used to reduce the energy consumption of mechanical pulping (Kure et al. 1999; Viforr & Salmén 2008; Salmi et al. 2012a). For example, mechanical pre-treatment of the wood can be implemented in the chipping process by adjusting the angle of the blade (Isaksson et al. 2013). The raw material can also be chemically pre-treated in order to reduce the energy consumption, especially sulphonation has been extensively studied (Atack & Heitner 1979; Westermark et al. 1987; Östberg & Salmén 1988; Heitner & Salmén 1994; Mao et al. 2004; Chagaev et al. 2005; Nelsson et al. 2017). This thesis includes studies of both chemical and mechanical pre-treatments.

In the Nordic countries, Norway spruce (*Pieca abies*) is the most common raw material for mechanical pulping. The structure of the wood fibres varies depending on the season due to variations in the rate of growth. In spring, the wood grows fast and needs good transfer capabilities for water and nutrients. This leads to wood fibres with thinner cell walls and large lumens, called earlywood (EW). Later on in

the year, the growth slows down and the fibres develop thicker cell walls and smaller lumens. These fibres support the trunk and branches, and are called latewood (LW). The transition from EW to LW is slow, and the fibres formed between these two stages are called transition wood. The transition from LW back to EW is abrupt, since growth stops during winter. One EW and one LW layer form an annual ring, which thus shows the growth of the tree's trunk cross-section area during one year. The significance of the two types of wood is that when the wood is compressed, the significantly softer EW absorbs most of the energy (Hickey & Rudie 1993; Murton et al. 2001; Huang et al. 2007), which means that the EW is over-refined while the LW remains poorly developed. Therefore, a better understanding of the material would provide new opportunities to utilize it more economically in the future.

Simulations have frequently been used to help develop the mechanical pulping process. For example, a combination of micromechanical and continuum modelling was used to analyse defibration in the mechanical pulping process (Holmberg 1998). In this research, the continuum modelling was used to study the initial breakdown of the wood and the micromechanical modelling was used to study the later stages of deformation. Wood deformation has also been modelled in order to develop a more energy-efficient defibration surface for the grinding process (Björkqvist 2002). Later, Fortino et al. (2015) used a micromechanical wood model to analyse the wood cell deformations, while Karlström & Eriksson (2014) developed a multi-scale model to study the material and energy balance of the refining process.

Wood is a viscoelastic material, so part of the mechanical energy that is used to deform the wood will be dissipated as heat energy. This means that a process in which as little energy as possible is dissipated as heat could achieve substantial energy savings. Numerical simulations are a promising approach to this issue, but there is currently no suitable model for the wood available. Most of the wood models that do exist are either wood continuum models, which are designed for construction applications with low temperatures and static loads, or they are micromechanical models.

1.2 Objectives and Scope

The hypothesis for this thesis is:

High-speed photography, image based experimental analysis and material modelling can be combined to study and simulate the difference in high strain rate compression behavior of earlywood and latewood.

The scope of this thesis is the modelling of the mechanical compression of wood for optimization of the mechanical pulping process. The objective of the thesis can be summarized by the following research questions:

Q1. What kind of compression models already exist, and how can a compression model for wood be developed that can adequately describe the behaviour of wood under rapid compression?

Q2. What kind of experimental data is needed to develop a material model for wood compression and how can the required experimental results be achieved?

In this work, the behaviour of wood under compression has been studied extensively, both by experimental work and material modelling. This thesis is limited to the radial compression behaviour of Norway spruce. Publication I presents a method for image-based analysis of the wood's behaviour, while Publication II presents the high strain rate and high temperature compression behaviour of native, chemically and mechanically pre-treated Norway spruce. These experimental results are used as the foundation for the wood compression models. Simple EW and LW compression models for the high strain rate compression of native and mechanically fatigued spruce at 20°C and 135°C are presented in Publication III. These compression models were developed into strain rate dependent, dynamic models in Publication IV, and the initial simulation results are compared with measured strain results in Publication V.

1.3 Outline and contribution

The EW and LW modelling requires full-field strain measurements during high strain rate compression. Full-field strain measurement techniques are presented in Chapter 2. High strain rate material testing in the split-Hopkinson pressure bar (SHPB) is discussed in Chapter 3. The complex compression behaviour of wood is summarized in Chapter 4 and state-of-the-art wood modelling techniques are described in Chapter 5. The various experimental methods and the chosen wood model are introduced in Chapter 6, and Chapter 7 presents both the experimental and modelling results. Chapter 8 presents a summary of the work and draws some conclusions about its significance.

The scientific contribution of this thesis can be summarized as:

- Development of an image-based method for the analysis of strain distributions in heterogeneous soft materials.
- Development of an image-based stress analysis method for the SHPB tests.
- Measurement of quasi-static and high strain rate experimental data on the radial compression of native and pre-fatigued Norway spruce.
- Development of EW and LW compression models for the radial compression of moist Norway spruce at 20°C, 100°C and 135°C.
- Development of dynamic (strain rate dependent) EW and LW compression models for the radial compression of moist Norway spruce at 20°C and 100°C.

1. Introduction

2 Full-field strain measurement

Alternative measurement techniques for full-field displacement measurements in solid mechanics are photoelasticity, the grid method, holography, speckle interferometry (SI) and digital image correlation (DIC) (Grédiac & Hild 2013). The two latter techniques, DIC and SI, are the most common methods used in wood compression tests, and these will be discussed in more detail below.

2.1 Digital image correlation

The basic principle of DIC is to record a series of images of the sample during deformation, and then to calculate the degree of displacement from the images. DIC can be used for both two-dimensional (2D) and three-dimensional (3D) analysis; one camera is enough for 2D analysis while 3D DIC requires two cameras that record the images simultaneously. The basic principle is the same for both techniques, so only 2D DIC will be presented here.

Any DIC implementation consists of three main steps: sample preparation, image recording and image processing. Standard DIC is best suited for strain measurements in which there are modest deformations of planar surfaces. The sample surface needs to have a random texture that does not have a specific orientation and is non-periodic (Sutton et al. 2009). This can be achieved with spray paint, for example. Only a digital camera and natural light, or a white light source, are needed for the recordings.

The image processing starts by dividing the image into subsets. The displacement is then calculated separately for each subset. The basic principle of DIC is to use cross correlation to identify the same subset in the images recorded both before and after the deformation. The correlation function is a function of 2D displacement and the location of the peak of the correlation function gives the position of the deformed subset. An iterative cross-correlation algorithm is needed for more complex deformation fields. Deformation of the subset can be accounted for by introducing a shape function that translates

the pixel coordinates in the reference subset into coordinates in the image after deformation. The grey values can be interpolated between the pixels in the image to achieve sub-pixel accuracy (Sutton et al. 2009).

2.2 Speckle interferometry

SI is a set of techniques that takes advantage of a two-beam interference pattern, involving at least one speckle wave and an optically rough surface (Grédiac & Hild 2013). Electronic speckle pattern interferometry (ESPI) can be used to measure both in-plane and out-of-plane displacements.

A speckle pattern is formed when an optically rough surface is illuminated with coherent light (laser) and the intensity of the image varies randomly. When a reference beam is superimposed on the speckle pattern, the fields interfere with each other and the resulting interferogram is also a speckle pattern. When interferograms recorded before and after deformation are compared, lines will occur where they are identical. The positions of these lines give information about the relative displacement (Wykes 1982; Petzing & Tyrer 1998).

2.3 From displacement to strain

The strain calculation from displacement data requires a compromise between filtering out noise and limiting the loss of mechanical data (Grédiac & Hild 2013). A popular method for estimating the strain from the displacement data is numerical differentiation. The drawback of this method is that it may amplify the measurement noise, but its accuracy can be improved by smoothing the displacement data before the differentiation (Pan et al. 2009a). This can be done, for example, by considering the displacement data nodes of strain elements.

The strain can also be calculated by Newton-Raphson iteration, or by similar algorithms. However, the error of the estimated strain limits such algorithms' use to local strains larger than 0.010 (Bruck et al. 1989). A pointwise, least-squares algorithm was used for strain estimation by Pan et al. (2009b).

2.4 Full-field strain measurement of wood

There have been several full-field strain measurements of wood based on DIC. The suitability of the DIC technique for testing small wood samples was evaluated by Choi et al. (1991), who found that the method was indeed suitable for the study of the properties of wood. They concluded that the DIC strain measurement results were in close agreement with both independent measurement results and finite

element method (FEM) analysis. Zink et al. (1995) scaled up the method, utilizing DIC on a series of increasing loads. These experiments revealed the development and mode of the failure, and captured the shift in the concentration of the strain in the wood samples during loading. Thuvander et al. (2000) used DIC to study crack tip strain fields on the annual ring scale in wood. DIC has also been used to study strain distribution along wood adhesive bonds (Serrano & Enquist 2005). Saari et al. (2009) used DIC to measure the strain distribution in wood's annual rings during compression tests in an SHPB. Vessby et al. (2010) used DIC to evaluate the strain distribution in a wood fibre-reinforced polymer lap joint and found the experimental, analytical and numerical results all to be in close agreement with respect to the strength and strain distribution.

Valla et al. (2011) compared ESPI to DIC for strain distribution measurements on mechanically stressed plywood samples. Although both methods yielded similar results, the DIC measurements were more detailed. In addition, an ESPI experimental set-up demands more experience than a DIC one, and the data acquisition is slower. DIC is, therefore, a more versatile method for strain analysis, but it has its own drawbacks. For example, it demands skilled sample preparation, and the post-processing and evaluation of the data is often more time-consuming than it is with ESPI.

The grid method is an image-based method where a grid is placed on the surface of the sample. The intensity profile of each grid line can be described with a periodical function. Phase maps can be evaluated from the images taken before and after deformation, and the difference in the phase field is proportional to the displacement field (Xavier et al. 2009). Xavier et al. (2009) studied the transverse and shear stiffness of wood using the grid method, and used a polynomial approximation scheme to estimate the strain fields.

2. Full-field strain measurement

3 The split-Hopkinson pressure bar

The SHPB is commonly used for the strain rate range that occurs in mechanical pulping (Gama 2004). It can be used to conduct high strain rate measurements of compression, torsion and tension. The tension and torsion devices are more complex than the compression device, the main differences being in the generation of the loading pulse, the specimen geometry and in how the sample is attached (Gray III 2000). Other material testing methods, such as the hydraulic testing machine used by Uhmeier and Salmén (1996a) to study radial compression behaviour of Norway spruce, tend to result in lower strain rates.

Hopkinson originally developed his pressure bar technique to measure the pressure produced by explosives (Hopkinson 1914). This technique was further developed by Davies (1948) and Kolsky (1949), so the SHPB bar is also known as the Kolsky bar. More details of the SHPB technique can be found in the review by Gama et al. (2004) and in the article by Gray III (2000).

3.1 The compression test technique

The SHPB consists of two elastic pressure bars: the incident bar and the transmitter bar. The sample is sandwiched between the bars during the measurement. The basic structure of the SHPB is presented in Figure 1.

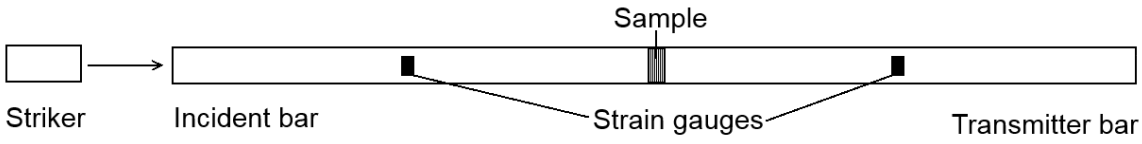

FIGURE 1 A schematic sketch of the SHPB set-up for compression tests.

A striker hits the incident bar and sends an elastic compression wave through the bar. This wave is then partially reflected at the interface of the incident bar and the sample, and is then partially transmitted through the sample, after which it is further transmitted from the sample to the transmitter bar. There is no reflection when the stress wave moves from a softer material to a stiffer material. Strain gauges on the bars record the incident, reflected and transmitted waves. These strain gauge recordings can be used to determine strain rate, strain and stress in the sample (Gray III 2000).

3.1.1 Stress and strain analysis

Stress and strain analysis of SHPB tests is based on the principle of one-dimensional wave propagation in an elastic material. The displacements and stresses can be calculated for any point by measuring the elastic wave at any point as it propagates along the bar. The strain rate of the sample can be calculated from the velocities at the faces of the incident and transmitter bars in contact with the sample, and the instantaneous sample length. The strain is then calculated by integration. The stress is calculated from the strain gauge measurement of the transmitted force divided by the instantaneous cross-sectional area of the sample (Gray III 2000).

Mohr et al. (2010) compared several formulas for calculating the non-uniform stress strain fields from dynamic experiments to the theoretical solution for waves in elastic samples. They found it important to avoid artificial time shifts. They also found that the best results for the most commonly used estimation methods were achieved by combining the estimate for the transmitter bar force-based stress with the average strain.

3.1.2 Image based stress analysis

An image-based stress analysis for the SHPB is proposed in Publication I. Two similar equations were presented for calculating the stress from the movement of the face of the transmitter bar in contact with the sample. Eq. 1 is based on the theory by Kolsky (1949) and Eq. 3 is based on a formulation presented by Mohr (2010). The subscript T in Eq. 1 and 3 refers to the transmitter bar, S is for the sample, and B is for the bar.

$$\sigma_T(t) = -\rho_B c_B \frac{\partial u_T(t)}{\partial t} \quad (1)$$

$$c = \sqrt{\frac{E_e}{\rho}} \tag{2}$$

$$\sigma_T(t) = -\frac{E_B A_B}{c_B A_S} \frac{\partial u_T(t)}{\partial t} \tag{3}$$

When the density in Eq. 1 is substituted according to the relation in Eq. 2, the only difference between Eq. 1 and 3 is the ratio of the cross-sectional area in Eq. 3. In Figure 2, the image-based stress pulses produced by Eq. 1 and 3 are compared to the strain gauge-based stress pulse.

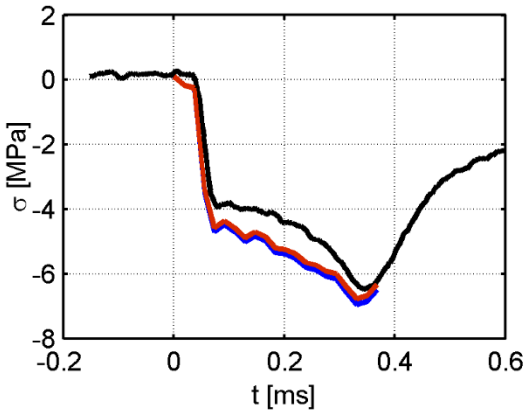

FIGURE 2 Image based stress pulses according to Eq. 1 (red) and Eq. 3 (blue) compared to strain gauge measurement (black).

3.2 Full-field split-Hopkinson measurement

The classic SHPB analysis only gives the average stress/strain relation. However, combining SHPB with image-based full-field methods provides the possibility to measure the local strain distributions and to derive the strain rate and the stress.

Grantham et al. (2004) used a combination of an SHPB and high-speed photography in order to perform high strain rate tension tests on disk shaped samples. Siviour (2009) used the combination of SHPB and high-speed photography to study the wave propagation in an SHPB. Gilat et al. (2009) used two high-speed cameras to obtain 3D displacement data from compression and tension tests in an SHPB.

Saari et al. (2009) measured the strain distribution in the annual rings of wood under compression using high-speed photography and DIC for displacement measurement in an encapsulated SHPB. They were

able to measure the strain fields for wet wood samples at the annual ring level. They showed that the method was suitable for evaluating the behavior of wood compression under conditions close to the conditions in a refining process.

3.3 Split-Hopkinson wood research

The challenge with SHPB testing of soft materials is the stress state equilibrium. The stress in the sample can be assumed to be in equilibrium after approximately three passes of the stress pulse through the sample (Davies & Hunter 1963). The number of transits of the stress pulse from one end of the sample to the other which are needed to achieve stress equilibrium can be approximated based on the ratio of the mechanical impedance between the sample and the bar material (Yang 2005). A constant strain rate implies that there is stress equilibrium in the sample (Gray III & Blumenthal 2000).

Many successful studies of wood have been presented using the SHPB. Bragov and Lomunov (1997) used it to study high strain-rate compression behaviour across and along the fibres of pine, lime and birch. Reid and Peng (1997) also used the technique to study the crushing strength of balsa, yellow pine, redwood, American oak and ekki along and across the fibres. In addition, Renaud et al. (1996a) used an SHPB to investigate the compression behaviour of aspen, birch and oak in all three principal directions. Moreover, Widehammar (2004) used the testing technique to study the radial, tangential and longitudinal compression behaviour of Norway spruce.

4 Wood properties

Norway spruce *(Picea abies*) is the most common raw material for mechanical pulping in the Nordic countries. Wood is an anisotropic material, meaning that its mechanical properties depend on the loading direction. The orthogonal directions of wood are tangential (T), radial (R) and longitudinal (L), and are presented for a wood sample in Figure 3 a and for an annual ring image in Figure 3 b. The longitudinal direction is along the fibres running in the direction of the length of the tree. The radial direction is perpendicular to the annual rings and the tangential direction is tangential to them.

The layers of the wood cell wall, starting from the outside of the cell are, primary wall (P), and the secondary wall (S). These are presented in Figure 3 c. The secondary wall in turn consists of three layers: the outer layer (S1), the middle layer (S2) and the inner layer (S3). Between wood cells is the middle lamella (M). The wood cell wall consists mainly of cellulose, hemicellulose and lignin. The microfibrils point in a slightly differently direction in the different layers of the cell wall. The angle between the microfibril and the length direction of the cell is called the microfibril angle. The microfibril angle is random in P, 45-90° in S1, 0-20° in S2 and 30-70° in S3 (Abe et al. 1991).

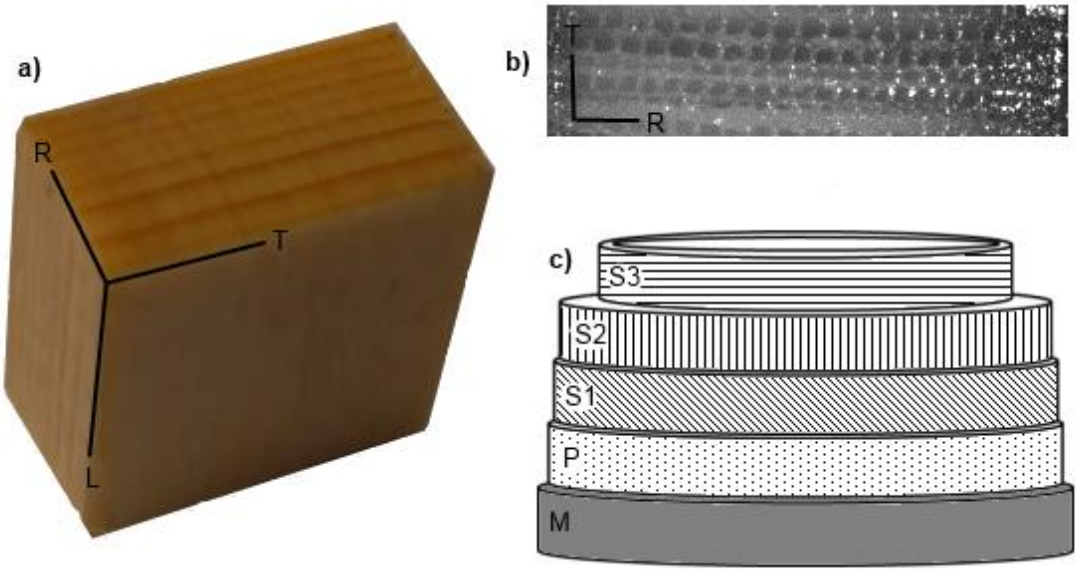

FIGURE 3 Images showing the orthogonal directions of wood **a)** for a spruce sample, **b)** an annual ring magnification image and **c)** the wood cell wall layers.

4.1 Wood compression behaviour

The stress strain curve for wood compression consists of three distinct parts: an initial elastic region, a plateau region and a densification region. For radial compression of wood, the elastic region corresponds to the reversible elastic deformation of the EW cells. For tangential and longitudinal compression, it is a combination of the response of both the EW and the LW cells. In the plateau region, the EW cells collapse, causing permanent damage to the wood cells. In the final stage, the collapsed EW cells are further compressed and some elastic compression of the LW may occur. The fundamental compression characteristics, i.e. the parts of the stress strain curve and cell collapse, are not affected by temperature (Tabarsa & Chui 2001; Law et al. 2006). The densification region also involves compression of the transition wood (Müller et al. 2003). The collapse of the LW cells may never occur, due to the thickness of the cell walls (Salmén et al. 1997; Tabarsa & Chui 2001). The Young's modulus is significantly larger in the longitudinal direction than in the radial and tangential directions (Bragov & Lomunov 1997; Widehammar 2004).

Strain rate, temperature and moisture content (MC) all have a major impact on the wood stiffness (Uhmeier & Salmén 1996a; Widehammar 2004). Therefore, it is essential to conduct experimental work under conditions which mimic the actual conditions created in the process under study (mechanical pulping) as closely as possible.

4.1.1 The impact of temperature on wood compression

Wood is significantly softened by higher temperatures. At a low strain rate, the plateau stress decreases linearly with an increase in temperature from 25 to 100°C (Uhmeier & Salmén 1996a; Salmén et al. 1997). The plateau stress levels out at 130-160°C. Any changes in the plateau stress, which occur at temperatures above 160°C are caused by chemical changes in the wood (Salmén et al. 1997; Uhmeier et al. 1998).

The yield strain does not change in the temperature interval 0-100°C. The yield stress drops by one tenth in the temperature interval 0-200°C during quasi-static radial compression (Uhmeier et al. 1998). During a series of quasi-static tests (Law et al. 2006), the Young's modulus for radial compression decreased by 84 % when the temperature was increased form 22°C to 140°C, the tangential compression decreased by 82 %, and it was 57 % for the longitudinal compression. For high strain rate compression, both the yield stress and the elastic modulus decreased as the temperature was raised (Salmi et al. 2012a). In Publication III, a reduction of 93 % in the Young's modulus was observed for high strain rate radial compression when the temperature was increased from 20°C to 135°C.

4.1.2 The impact of strain rate on wood compression

The strain rate is known to have an impact on the compression behaviour of wood, and the wood's MC affects its response to different strain rates. When comparing low and high strain rate compressions, the difference in the Young's modulus is low for dry wood, but it is more significant for wood that is saturated with water. Under low strain rate compression, the Young's modulus is lower for water-saturated wood than it is for dry wood. However, at a high strain rate, the water-saturated wood can sometimes be stiffer than dry wood (Renaud et al. 1996b). The stress in the plateau region increases greatly with an increasing strain rate, especially for water-saturated wood (Uhmeier & Salmén 1996a). The difference in compression behaviour between low and high strain rates is more significant for fully saturated wood than it is for fibre-saturated wood, this being due to the slow transportation of free water in the lumens in the saturated wood (Widehammar 2004).

4.2 Earlywood and latewood

The differences in the mechanical properties of wood fibres is one of the challenges in mechanical pulping. During compression, the EW fibres can be crushed while the LW fibres remain intact. Local compression behaviour is therefore important. The majority of wood research has focused on its bulk properties, but there has been very little research into variations in the fibres within one annual ring.

EW is anisotropic with regard to both transverse shrinkage and transverse elasticity, while LW is almost isotropic in the transverse direction (Boutelje 1962). Both the radial and tangential Young's moduli

increase curvilinearly with increasing density (Watanabe et al. 2002). The Young's modulus increases with annual ring number and the height of the tree while the shear modulus increases according to the ring number, but decreases with the height. The percentual variation in the Young's modulus is nearly as great within one annual ring as it is across all the rings from the heart of the wood to its outermost ring (Cramer et al. 2005). There are other key differences between EW and LW. In tensile loading, the strain amplitudes in EW can be twice as large as the strain amplitudes in LW (Jernkvist & Thuvander 2001; Eder et al. 2009), while their Poisson's ratio also differs (Oscarsson et al. 2012).

Strain rate and temperature do not have a significant effect on the distribution of strain between EW and LW. The temperature increases more slowly in LW, and Hickey & Rudie found that the final temperature was lower in LW than it was in EW (Hickey & Rudie 1993). The difference in the softening temperatures for EW and LW is not dependent on measurement frequency (Wennerblom et al. 1996).

Farruggia and Perré (2000) studied the elasticity of Norway spruce by performing both microscopic tensile tests and numerical simulations. According to their results, the Young's modulus was 744 MPa for EW in the radial direction and 210 MPa in the tangential direction. For LW, on the other hand, the Young's modulus was found to be 1230 MPa in the radial direction and 1250 MPa in the tangential direction. All their tests were performed at room temperature using wood samples with 7 % MC. Farruggia and Perré surmised that the error in their radial LW measurement could be caused by mechanical coupling, since the EW close to the measurement area caused shear and normal stresses in the tangential direction. The experiment was also expected to include the contributions from friction and Poisson constriction. These results are in line with Bouteljes' (1962) finding that EW is anisotropic while LW is close to isotropic in the transverse direction.

The location of the maximum strain is about one fourth of the way into the annual ring (Jernkvist & Thuvander 2001; Hassel et al. 2009). Initial cell wall buckling has been observed from three to ten rows of cells in from the edge of the annual ring (Müller et al. 2003). The EW lumens collapse row by row in two different modes: the cell walls in the loading direction either tilt or bend sharply, taking on an s-shape. The s-shape bending causes more plastic deformation than when the cell walls are tilted. LW compression consists of the flattening and lateral expansion of the cells up to 35 % strain, and s-shape deformation of the cell wall above that (Dumail & Salmén 1996). These results have also been confirmed by simulations (Fortino et al. 2015).

4.3 Wood fatigue

The accumulation of fatigue damage in wood starts with the crack initiation, which then proceeds through micro-crack formation to the formation of macro-cracks. Shear is the most effective way of causing micro-cracks in the fibres. These are formed after roughly 3000 radial compression cycles, after which the cracks accumulate at a similar rate as they do in shear. Tensile loading has little effect on the

damage accumulation (Hamad & Provan 1995). When the objective of the process is to achieve large deformation with low energy consumption then a two stage loading with a combination of compression with low shear first, followed by plain compression, is more beneficial than simply using compression (De Magistris 2005). The structural breakdown of wood is favoured by a higher temperature and a lower compression frequency (Salmen et al. 1985; Salmen 1987). Although no parallel cracks or delamination can be seen with an optical microscope after cyclic radial compression, there is a slight weakening of the structure at the corners of the cells. This might be due to micro-cracks smaller than 10 nm in width (Bergander & Salmen 2000).

Pre-fatigued wood is not very sensitive to the loading direction, the biggest difference between native and pre-fatigued wood being for the radial loading (Miksic et al. 2013). Pre-fatigue treatment also reduces the thermal conductivity of wood (Mauranen et al. 2015).

A layer of fatigued wood fibres is generated during the grinding process (Salmi et al. 2011). A pre-fatigue treatment can reduce the specific energy consumption needed for mechanical pulping (Kure et al. 1999; Viforr & Salmén 2008; Salmi et al. 2012b).

4. Wood properties

5 Wood modelling

Wood material models can be divided into two main groups: micromechanical models that model the details of the wood's structure, and continuum models that model the wood's overall behaviour. There are several micromechanical wood models, but they can only be used at the specific scale level. A model that consists of different scale levels is called a multiscale model, and such a model is needed in order to fully understand the mechanical behaviour of wood (Mishnaevsky Jr. & Qing 2008). There are fewer wood continuum models.

5.1 Micromechanical models

One of the most popular micromechanical models is the honeycomb model presented by Gibson and Ashby (1997). Gibson and Ashby presented a hexagonal honeycomb model and compared their predictions for transverse elastic moduli as a function of relative density with experimental data. The behaviour of wood until the first fracture was investigated with a honeycomb model built of hexagonal cells by Ando and Onda (1999). A similar honeycomb model with hexagonal cells was used by Moden (2008), who developed a two-phase honeycomb model that was divided into EW and LW via different relative densities. The results of the two-phase model were significantly more accurate than the ones achieved with a one-phase model.

There are also models that take the structure of the cell wall into account. Saavedra Flores (2011) stated that the microfibril angle is the most important parameter controlling the balance between stiffness and flexibility in trees. Saavedra Flores studied the recovery of wood in loading-unloading cycles with a three-scale FEM model of the cell walls. This was able to capture the recovery mechanism at the cell wall level and could accurately reproduce the characteristic stiffening of the cell wall when the microfibril angle in the cell wall is decreased.

The cell wall has been modelled with two layers (Cave 1976) and three layers (Yamamoto 1998). Cave divided the cell wall into S2 and a binding layer. Cave assumed that the lignin concentration in the secondary wall is uniform and that only the thickness of the secondary wall's S2 layer accounts for the varying thicknesses of the cell walls. The model bases the relative cell wall layers' thickness on basic density or total cell wall thickness. The error in the calculated longitudinal shrinkage was lower when the relative thickness of the cell wall layers was considered (Cave 1976). Yamamoto developed a three-layer model with the middle lamella, S1 and S2. The strain caused by the microfibril angle was modelled better when both the lignin swelling and the cellulose tension were taken into account. (Guitard et al. 1999) improved Yamamoto's three-layer model by replacing Yamamoto's condition that the integral of the stress equals zero with the condition that the stress equals zero everywhere.

Koponen et al. (1989; 1991) combined the honeycomb with cell wall modelling. They started by modelling the cell wall with a three-layer model (Koponen et al. 1989) and then developed models based on the structure and elastic properties of the cell wall. The models used three groups of regularly shaped cells: EW cells, LW cells and ray cells. A comparison of six different models was used to define the global elastic properties of the wood material. However, the models had different radial cell wall angles and S2 microfibril angles, and two of them left out the ray cells completely (Koponen et al. 1991).

Hofstetter et al. (2005) developed a micro elastic model, based on a four-step homogenization scheme. The steps are polymer network, cell-wall material, softwood and hardwood. Their model overestimates the longitudinal normal stiffness and underestimates the transverse normal stiffness. The reason for this is the assumption that the microfibril angle is zero. This is also believed to be the reason for the shear moduli being significantly underestimated. The model also overestimates the shear stiffness, presumably due to the simplification of the cell lumen and other vessels, which were represented by cylinders.

Persson (2000) conducted multiscale modelling of wood, starting from the chemical components of the cell wall and ending with the average mechanical properties of an annual ring. The cell wall properties were calculated from the known properties of the main components of the cell wall. The properties of the wood fibre and the wood structure were then calculated using two different cell models.

Fortino et al. (2015) presented 3D micro-FEM simulations using a five-layer model for the wood cell wall in combination with hexagonal cells. They simulated two loading cases, one using compression and the other using a combination of compression and shear. They then compared their results with experimental data.

5.2 Continuum models

Adalian and Morlier (2001) studied wood under static and dynamic multiaxial compression and presented a wood continuum model. They compared their wood model based on the hypo-elastic law with a traditional elasto-plastic model and found that the simulation results based on the hypo-elastic law were more realistic than the results obtained with the elasto-plastic model.

Holmberg (1998) used both micromechanical and continuum models to study wood defibration. For the continuum model, Holmberg divided the material into EW and LW. A crushable foam plasticity model divided into several layers was used for the EW, while the LW was modelled as a linear elastic material.

Björkqvist (2002) and Björkqvist et al. (1999) modelled wood as a simple, linear Voigt-Kelvin solid. Their model was used for simulations aimed at optimizing the deformation and temperature development involved in the fatigue work in the wood-grinding process. The simulated temperature profile near the grinding stone was very similar to the corresponding experimental profile. However, at greater distances, the simulated pressure profile differed significantly from the measured pressure profile.

Hanhijärvi and Mackenzie-Helnwein (2003) developed a material model for the analysis of wood in the transversal plane. This 2D model was based on a thermodynamically consistent hyperelastic formulation. The model defines a decomposition of the total strain into the sum of several strain tensors associated with different deformation mechanisms. The model includes irrecoverable deformations with a plastic element.

Milch et al. (2016) used an elasto-plastic material model for simulations of wood joints. They achieved good agreement between the experimental results and their simulations. The simulated results for Norway spruce only differed by about 10 % from the experimental results. Elasto-plastic wood models were also presented in (Kollman & Côte 1968).

5. Wood modelling

6 Materials and methods

6.1 Material testing

The raw material for the compression tests was fresh Norway spruce from roughly 80-year-old trees from Myrskylä in southern Finland. The logs were sawn into smaller pieces and stored in a freezer. Some of the samples were mechanically pre-fatigued and some were chemically treated. The sample surface was cut with a microtome before the measurements. Some samples were also spray painted to get a better texture for the image correlation. The main steps of the sample preparation are presented in Figure 4.

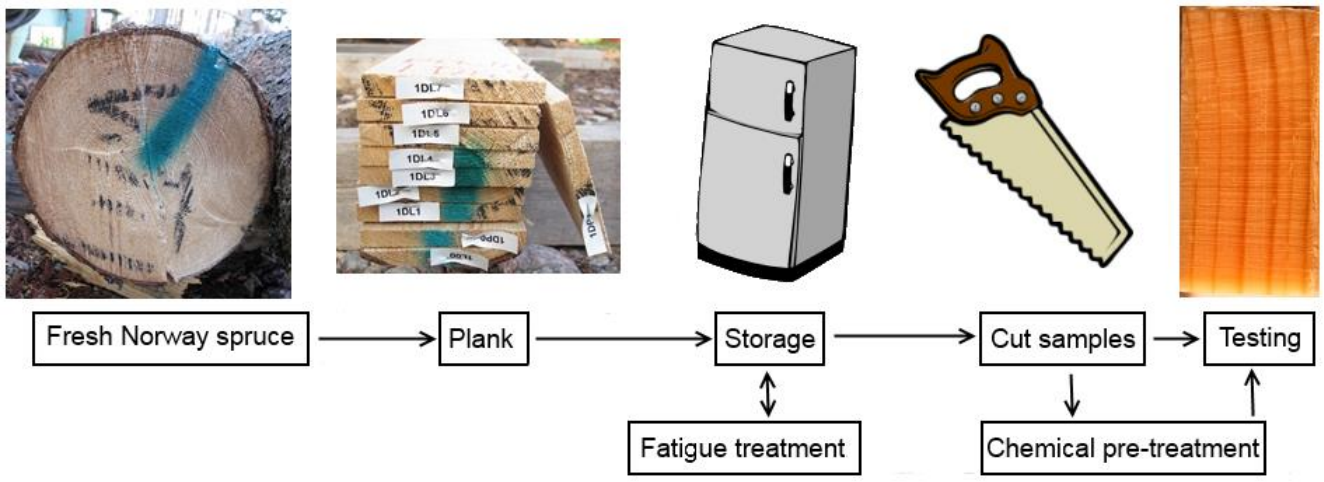

FIGURE 4 Diagram showing the most important steps of the wood sample preparation.

The mechanical pre-fatigue treatment was applied by the device presented in (Lucander et al. 2009; Salmi et al. 2009), with 20 000 strain pulses at 500 Hz. This can be considered an intensive fatigue treatment. The chemical pre-treatment chosen was sulphonation. The sulphonation was carried out with impregnation liquids containing 20 g/L sodium sulphite (Na_2SO_3) and pH 4 and 9, which was adjusted with sulphuric acid. The samples were pre-heated at 105°C for 10 minutes and then immersed into the cold impregnation liquid for 15 minutes. The excess solution was then drained and the samples were heated to 130°C for 5 minutes (Logenius et al. 2013; Engberg et al. 2014). The theoretical sulphite charge in the wood was 4 %.

6.1.1 Quasi-static material testing

The quasi-static measurements were conducted in an Instron E1000 tensile testing machine at Aalto University in Espoo, Finland. A heated water bath was used for measurements at 80°C (could not be heated to 100°C for safety reasons). Measurements at room temperature were conducted both in the air and under water. For the underwater tests, water was circulated in front of the sample to remove air bubbles from the cell lumen. The set-up used for the quasi-static measurements is presented in Figure 5.

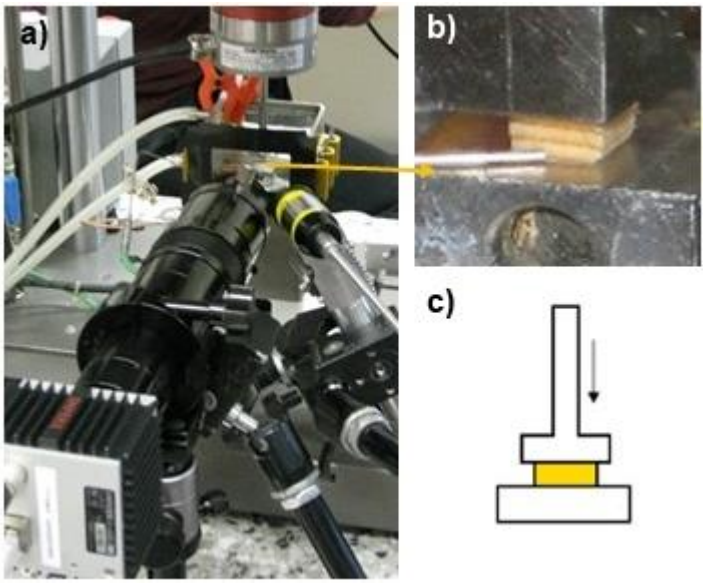

FIGURE 5 Images of a) the setup for the quasi-static measurements with the water bath b) a close-up of the sample in the testing machine and c) a schematic sketch showing the working principle of the testing machine.

An Infinity K2 long distance microscope was mounted on an Imperx Lynx GigE camera for the quasi-static measurements. The camera captured images at 2 Hz during the compression. A Cavilux HF pulsed diode laser (effect 500 W and wavelength 808 nm) was used for illumination. The camera with the long distance microscope and the laser optics can be seen in Figure 5 a.

6.1.2 High strain rate material testing

The high strain rate measurements were conducted in an SHPB at Mid Sweden University in Sundsvall, Sweden. The device was encapsulated in an insulated pressure vessel (Holmgren et al. 2008), and could therefore be heated with saturated steam to 135°C. The SHPB measurement set-up is presented in Figure 6.

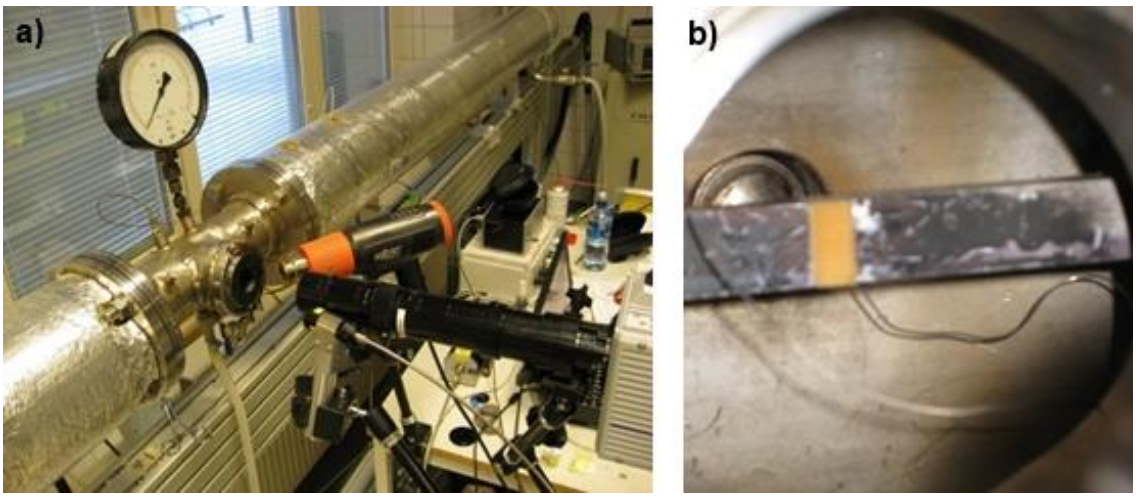

FIGURE 6 Images of a) the encapsulated SHPB and b) the sample sandwiched between the SHPB bars.

Two configurations of the long distance microscope were used for the high strain rate measurements, fibre magnification and annual ring magnification. The microscope was mounted on a Photron SA5 high-speed camera. The system captured images at 50 000 Hz and 100 000 Hz, depending on the magnification used. The illumination was provided by the same laser as was used in the quasi-static measurements. The long distance microscope and the laser optics can be seen in Figure 6 a. Behind the long distance microscope in Figure 6 a is a heater, which was used to demist the window in the encapsulation of the SHPB.

6.1.3 Measurement plan

Two types of measurements were conducted: quasi-static measurements at strain rate 0.004 s^{-1}, and high strain rate measurements at 800-2400 s^{-1}. The quasi-static measurements were conducted at both room temperature and 80°C, while the high strain rate measurements were carried out at 20°C, 100°C and 135°C. The samples were native Norway spruce, mechanically pre-fatigued Norway spruce and chemically pre-treated Norway spruce. A flow diagram showing the measured combinations is presented in Figure 7. The aim was to obtain four good measurements for each of the set-ups, although some of the measurements could not be analysed due to water spraying out of the sample.

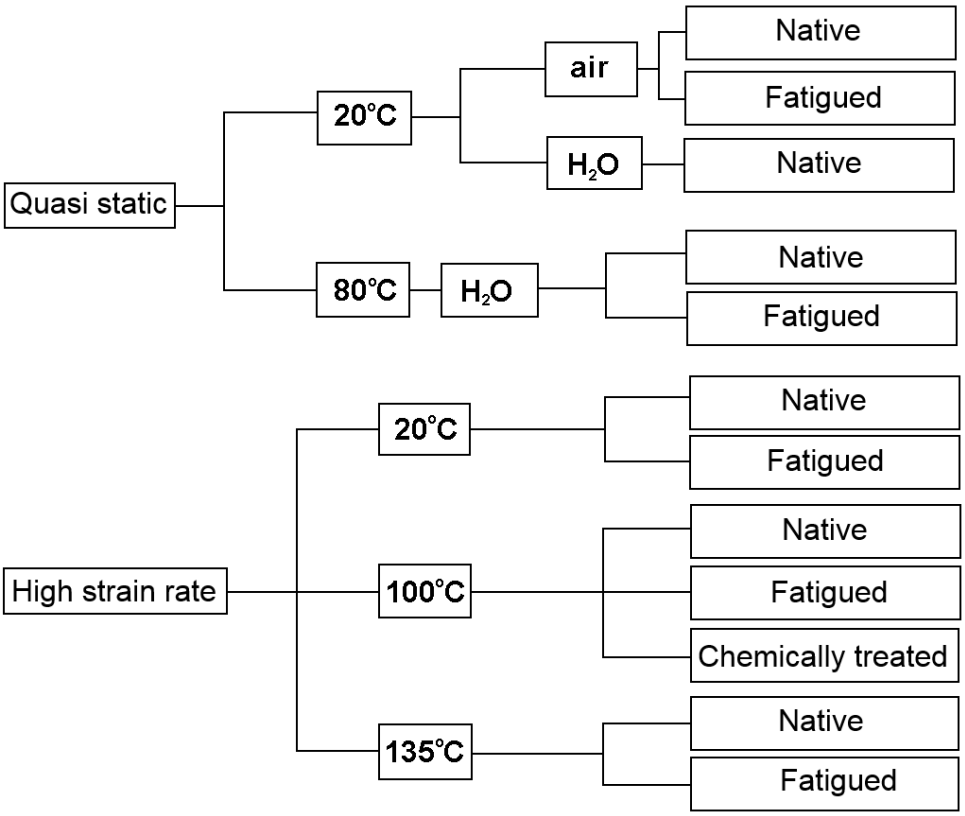

FIGURE 7 A flow diagram showing the quasi-static and high strain rate measurement temperatures and samples.

6.2 Image-based strain analysis

An image-based strain analysis method was presented in Publication I. An earlier version of the image based stress and strain method was presented in (Moilanen et al. 2014). The DIC was implemented by the standard cross-correlation technique in Davis 8 (LaVision), which is also used for particle image velocimetry (PIV). More information on PIV techniques is presented in (Raffel et al. 2007). As in all DIC methods, the frame was divided into subsets and the displacement between two sequential images was calculated with the chosen correlation technique. The PIV correlation technique gave a correlation result for all the textures in a subset with sub-pixel accuracy, and the displacement is the most probable value for the subset. Other DIC methods trace a fixed texture and give the displacement for the central nodal point. The PIV correlation technique gives a better result when part of the texture disappears between images. PIV based strain measurement was also used by White (2003) and Lee (2006).

The size of the subset is a compromise between resolution, calculation uncertainty and calculation time. The subset size needs to be as small as possible to improve the spatial resolution, but too small a subset increases the uncertainty of the calculated displacement. Increasing the overlap between the subsets increases the spatial resolution, but does not provide any new data, since the data of overlapping subsets are correlated. For the high strain rate data, the size of the subsets was 64 × 64 pixels for the first pass and 16 × 16 pixels for the second pass, and for the quasi-static data it was 32 x 32 pixels. Both passes were made with a 50 % overlap of the subsets, which gave a distance of 8-16 pixels between grid points. Only small displacements are allowed between the frames for the DIC, and this was achieved by adjusting the frame rate.

The displacement data was used to calculate the movement of the grid points distributed over the sample. The central nodal points of the subsets in the displacement analysis were chosen as grid points. The number of grid points ranged from 1024 to 2024. In the first frame, the points were evenly distributed. The positions of the grid points were updated according to the displacement data. The displacement analysis was conducted for the whole frame since the whole sample moved slightly during the compression.

The local strain was calculated by numerical differentiation, considering the grid points as the nodes of 4-node quadrilateral elements. Dahl (2009) presented a method to calculate all three in-plane strain components by a formulation that is commonly used in finite element analysis and Thuvander (2000) used triangular elements for the shear strain calculation. Eq. 4–6 were used to calculate the in-plane strain components.

$$\varepsilon_{RR} = \frac{\partial u}{\partial R} \tag{4}$$

$$\varepsilon_{TT} = \frac{\partial v}{\partial T} \tag{5}$$

$$\varepsilon_{RT} = \frac{1}{2}\left(\frac{\partial u}{\partial T} + \frac{\partial v}{\partial R}\right) \quad (6)$$

6.2.1 Earlywood and latewood strain

The radial direction of the wood was not always parallel to the compression direction x in the image. The difference between the directions has been taken into account, since the EW and LW analysis is based on the average radial strain in the tangential direction. The strain data is stored in a matrix and the direction was corrected by inserting empty spaces into the matrix at the beginning and end of each row (x direction). The amount of empty spaces depends on how oblique the sample was. This gave a good approximation as long as the angle between the x and radial directions remained small.

The EW and LW analysis start with calculating the average ε_{RR} in the tangential direction. The average strain was plotted as a function of the radial position. The EW and LW contributions were identified from the curve; LW from the maximum values and EW from the minimum values.

6.3 Wood modelling

For the mechanical pulping application, the micromechanical compression behaviour is not so important, but the large-scale fatigue development is. So, a continuum model was chosen for this application. The model was divided into EW and LW, due to the significant difference in their stiffness.

6.3.1 Static and dynamic model

Two similar but fundamentally different wood models have been developed. In Publication III, a compression model was presented that did not take the strain rate explicitly into account (the model is only accurate at the strain rate of the measurement).

$$\sigma_{LW} = E_{LW}\varepsilon_{LW} \quad (7)$$

$$\sigma_{EW} = \begin{cases} E_e^{EW}\varepsilon_{EW} \\ E_e^{EW}\varepsilon_y^{EW} + E_p^{EW}\left(\varepsilon_{EW} - \varepsilon_y^{EW}\right) \\ E_e^{EW}\varepsilon_y^{EW} + E_p^{EW}\left(\varepsilon_d^{EW} - \varepsilon_y^{EW}\right) + E_d^{EW}\left(\varepsilon_{EW} - \varepsilon_d^{EW}\right) \end{cases} for \begin{cases} \varepsilon_{EW} \le \varepsilon_y^{EW} \\ \varepsilon_y^{EW} < \varepsilon_{EW} \le \varepsilon_d^{EW} \\ \varepsilon_{EW} > \varepsilon_d^{EW} \end{cases} \quad (8)$$

In publication IV, the compression model was developed into a dynamic model by adding the strain rate-dependent term $\eta\dot{\varepsilon}$.

$$\sigma_{LW} = E_{LW}\varepsilon_{LW} + \eta^{LW}\dot{\varepsilon}^{LW} \quad (9)$$

$$\sigma_{EW} = \begin{cases} E_e^{EW}\varepsilon_{EW} + \eta^{EW}\dot{\varepsilon}^{EW} \\ E_e^{EW}\varepsilon_y^{EW} + E_p^{EW}\left(\varepsilon_{EW} - \varepsilon_y^{EW}\right) + \eta^{EW}\dot{\varepsilon}^{EW} \\ E_e^{EW}\varepsilon_y^{EW} + E_p^{EW}\left(\varepsilon_d^{EW} - \varepsilon_y^{EW}\right) + E_d^{EW}\left(\varepsilon_{EW} - \varepsilon_d^{EW}\right) + \eta^{EW}\dot{\varepsilon}^{EW} \end{cases} for \begin{cases} \varepsilon_{EW} \le \varepsilon_y^{EW} \\ \varepsilon_y^{EW} < \varepsilon_{EW} \le \varepsilon_d^{EW} \\ \varepsilon_{EW} > \varepsilon_d^{EW} \end{cases} \quad (10)$$

6.3.2 Modelling of fatigue behaviour

The compression of mechanically fatigued wood showed an additional section in the stress strain curve where the pre-fatigued EW fibres collapse. There are two alternatives when modelling this additional section: to add a linear term to the model or let it reduce the elastic modulus (E_e) of the elastic region of the stress strain curve. The first approach was used at room temperature in Publication III, and the second at a high temperature in Publication III and in all cases in Publication IV. The advantage of this additional term is that it gives more information about the compression process, and the advantage of reducing E_e is that it simplifies the simulation of the transition from native to fatigued wood. The alternative models are shown in Figure 8.

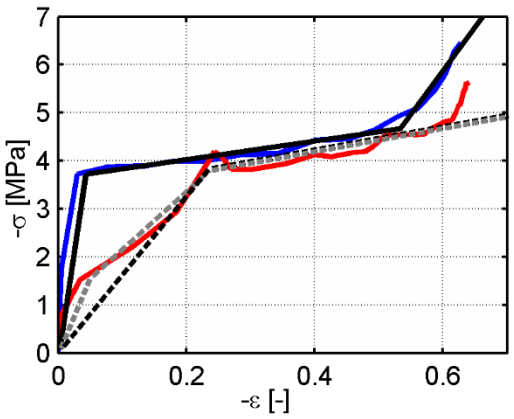

FIGURE 8 Measured EW stress strain curves of native (blue) and fatigued (red) wood and the alternative modelling approaches: native model (black solid line), fatigued with reduced Ee (black dashed line) and fatigued with additional term (grey dashed line).

7 Results

Both image-based data and reference data were gathered for all the compression tests. For the SHPB compression tests, the stress and strain analyses were verified by comparing the image-based and the strain gauge-based results. The image-based strain and strain gauge-based stress were chosen for further analysis, since they were considered the most accurate. For the quasi-static compression tests, the image-based average strain was compared to the strain measured by the Instron E1000.

7.1 Compression mechanisms

The images captured during the compression show what happens during the compression, especially the images captured with fibre magnification. The images can be related to a specific point on the stress strain curve. Fibre magnification images captured during high strain rate compression of native and fatigue wood at room temperature and 135°C were presented in Publication III. Figure 9 a shows the high strain rate stress strain curve from the compression of one native and one fatigued-tested sample at room temperature. The circles mark the positions of the images in Figures 9 b-d and Figure 10. The arrows indicate the direction of the compression in Figure 9 b-d and Figure 10.

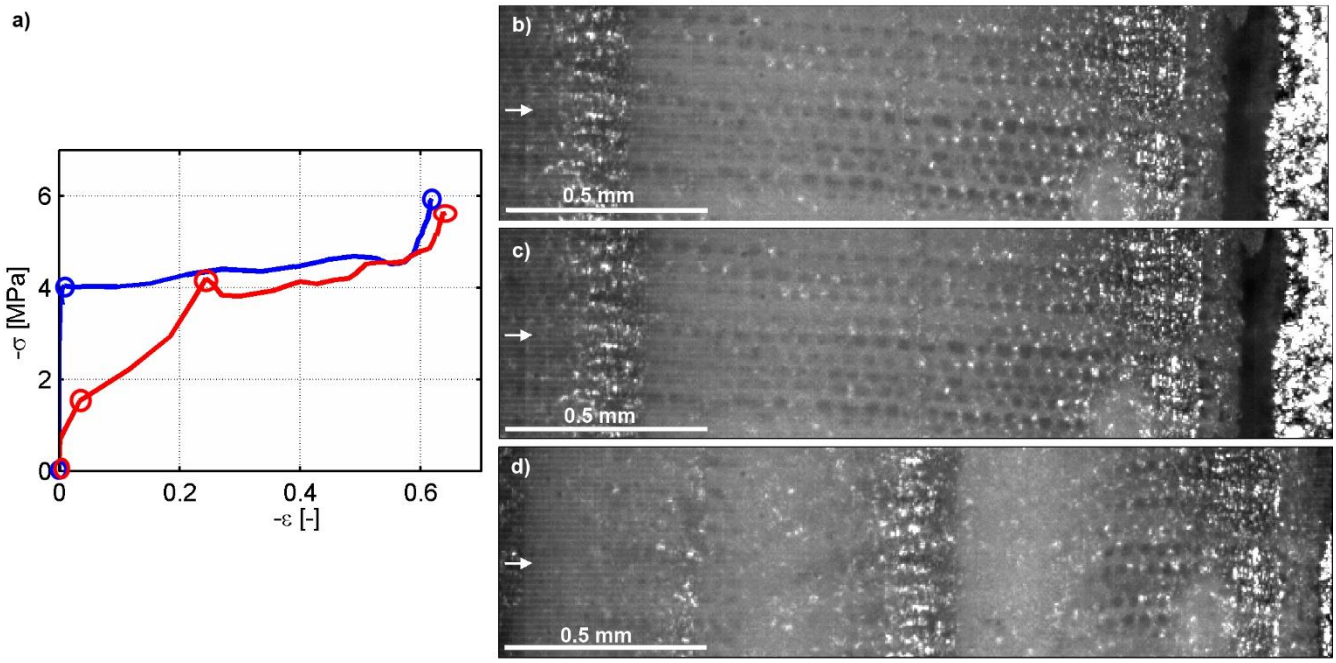

FIGURE 9 The high strain rate room temperature a) EW stress strain curves for the compression of native (blue) and fatigued (red) wood and images of native wood captured b) before compression, c) at the yield limit and d) in the end of the compression.

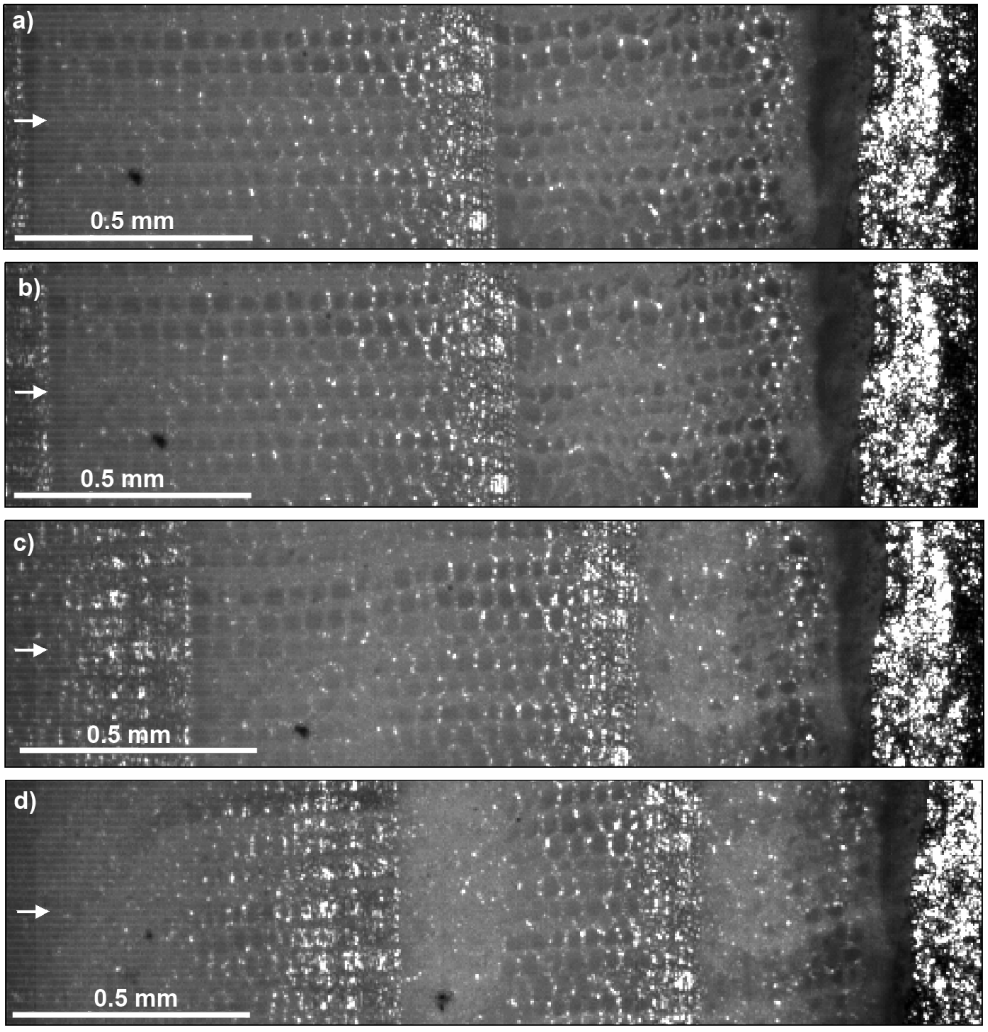

FIGURE 10 Images of fatigued wood during high strain rate compression at room temperature captured a) before compression, b) at the end of the elastic compression c) at the yield limit and d) at maximum compression.

For the native sample in Figures 9 b-d, we can see that the EW cells collapse after the yield limit. For the fatigued sample in Figure 10, the EW cells start to collapse before the yield limit. It is assumed that the cells that collapsed are those, which have been softened by the pre-fatigue treatment.

The compression can be considered to be mainly a progressive collapse of the EW. The strain rate is locally high, compared to the average of the sample when the annual ring collapses. The difference between one annual ring and the whole sample was presented in Publication I and is shown in Figure 11, where the strain is plotted as a function of time for one annual ring (from fibre and annual ring magnification samples) and the average of all the EW in the sample.

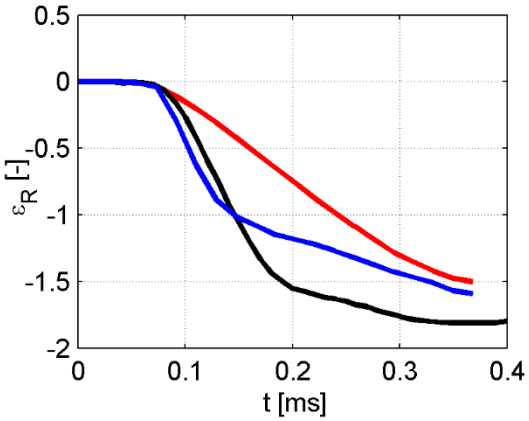

FIGURE 11 EW strain as a function of time for one annual ring of a sample (blue) average of all annual rings of a sample (red) and one annual ring from fibre magnification measurement (black).

The fatigue development in wood was studied in a quasi-static cyclic compression test. By comparing images from subsequent compressions, it is clear that the sample collapses in exactly the same way when it is compressed to the same strain level again. The EW stress strain curve is presented in Figure 12 a and the images captured at the marked positions are shown in Figures 12 b and c. The arrows indicate the direction of the compression in Figures 12 b and c.

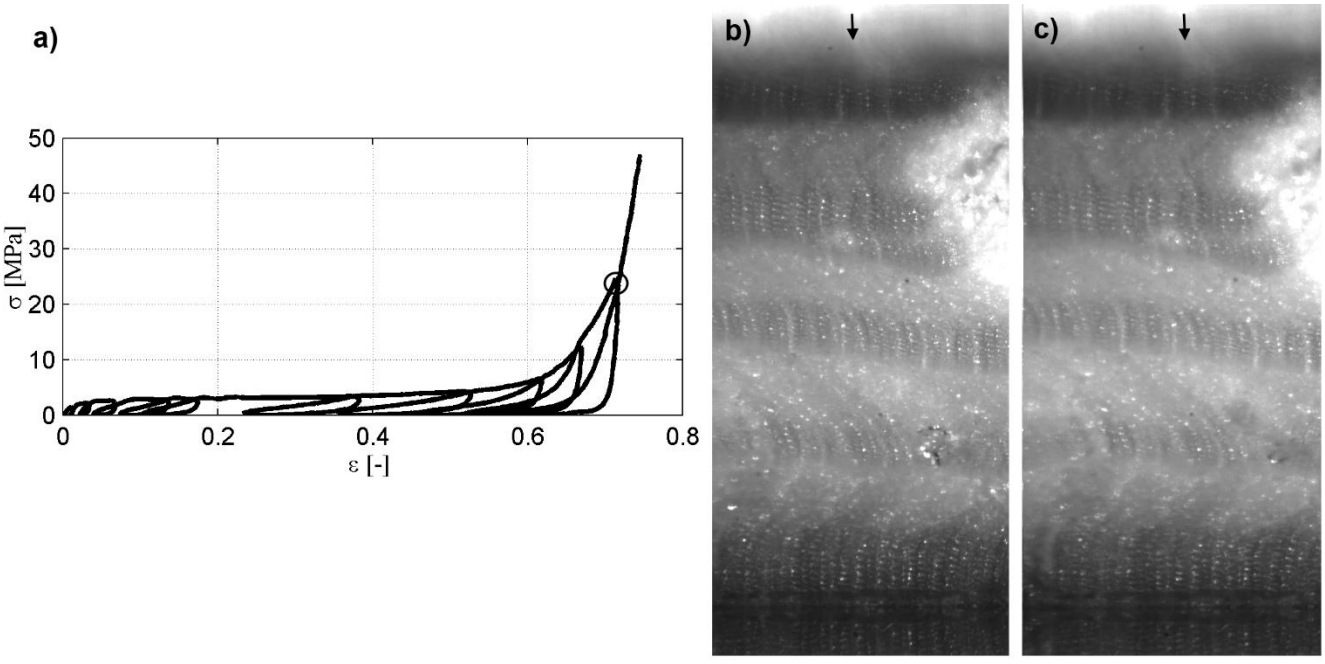

FIGURE 12 The quasi-static cyclic compression a) EW stress strain curve and images from b) the first pass and c) the second pass of the marked position.

Figure 12 a also shows that the sample did not completely relax between the compressions. This can either be the result of insufficient relaxation time or plastic changes in the sample. More results from the cyclic compression test are presented in Publication IV.

7.2 Stress strain curves

EW and LW stress strain curves were extracted from the full field measurement data. High strain rate stress strain curves for average wood, EW and LW at high temperature were presented in Publication II. The high strain rate EW stress strain curves in Figure 13 show that the wood is significantly stiffer at room temperature than at 100-135°C (note that the scale of the stress axes differs). The chemical pre-treatment did not decrease the elastic modulus for EW, but the plateau stress was slightly reduced for the samples treated at pH 9. Fatigued wood tested at 100°C was approximately as soft as native wood at 135°C and it seems that the mechanical fatigue treatment only had a slight effect when the sample was compressed at 135°C.

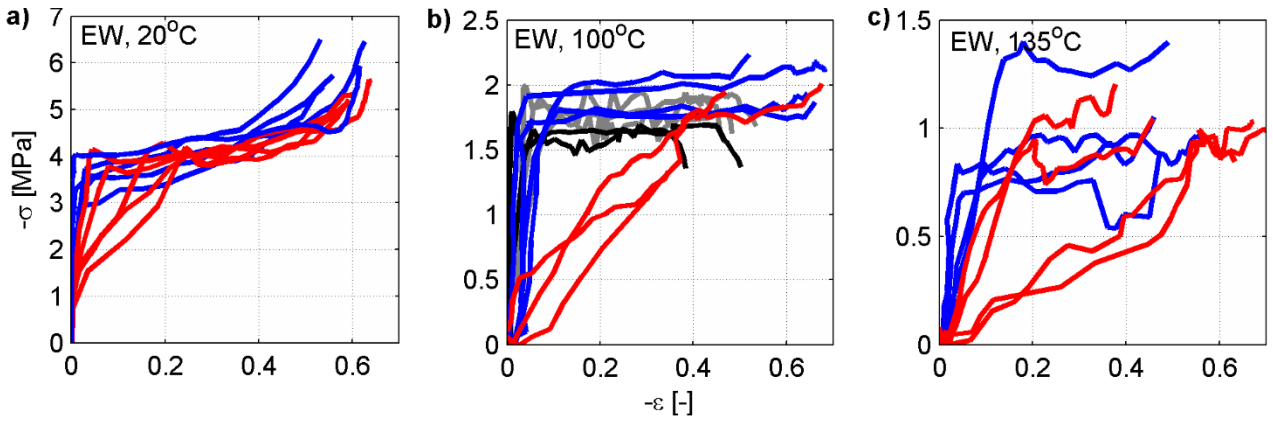

FIGURE 13 High strain rate EW stress strain curves for native wood (blue), mechanically pre-fatigued wood (red) and chemically treated wood (pH 4 gray and pH 9 black) tested at a) 20°C, b) 100°C and c) 135°C.

The LW curves in Figure 14 shows that LW compression is not significantly affected by chemical or mechanical pre-treatments, nor did the increased temperature have a significant effect on LW compression.

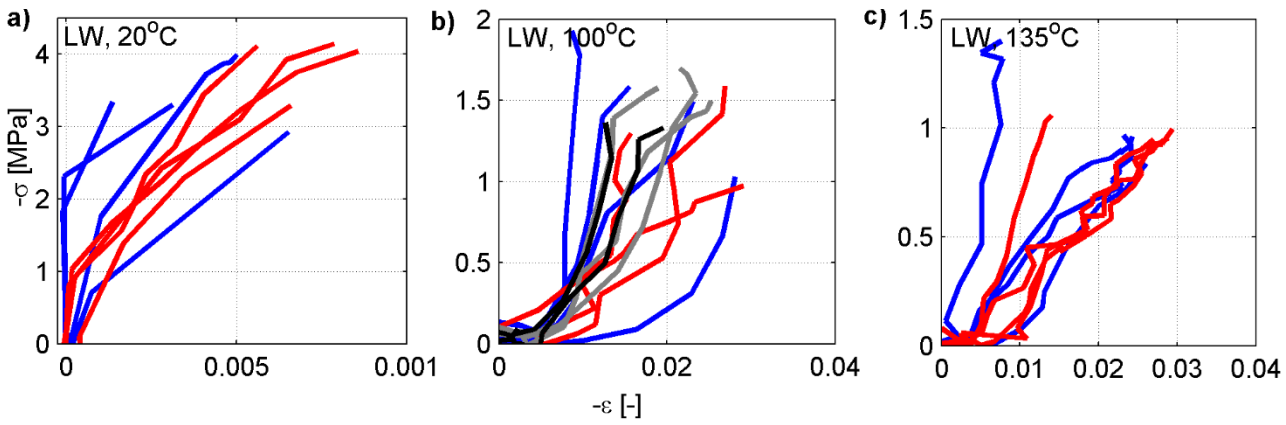

FIGURE 14 High strain rate LW stress strain curves for native (blue), mechanically (red) and chemically (pH 4 gray and pH 9 black) treated wood tested at a) 20°C, b) 100°C and c) 135°C.

7.3 Wood compression model

Three different kinds of samples were tested: native wood, mechanically pre-fatigued wood and chemically pre-fatigued wood. Based on the initial results presented in Publication II, the mechanical pre-treatment was more effective than the chemical pre-treatment. This can also be seen in Figure 13 b. The mechanical fatigue is also more interesting from the process point of view, so only native and mechanically pre-treated samples are modelled.

The compression models presented in Publication III did not explicitly take the strain rate into account, and the models are thereby only accurate for the strain rate of the measurement. They are, however, appropriate for modelling the mechanical pulping process since the strain rate was chosen accordingly. The compression models also provides numerical values for the material parameters that can be compared for the different conditions (temperature and fatigue). The compression models at 135°C were improved and the material parameters for compression at 100°C were fitted to measurement data after Publication III, and are presented in (Moilanen et al. 2015). The experimental data compression models for EW are presented in Figure 15 and the experimental data and compression models for the LW in Figure 16.

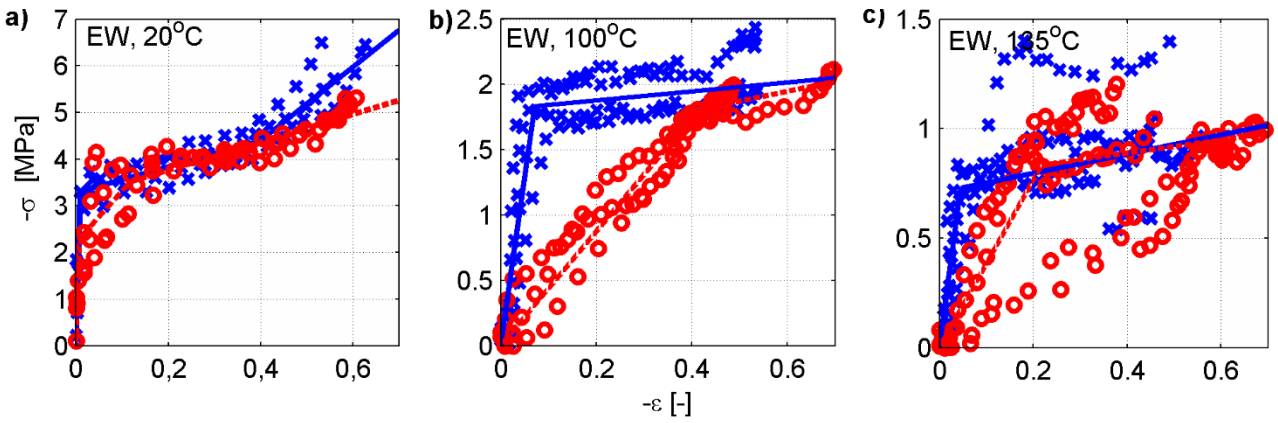

FIGURE 15 Measurement data and compression model for native (blue **x** and solid line) and fatigued (red **o** and dashed line) EW from high strain rate tests at a) 20°C, b) 100°C and c) 135°C.

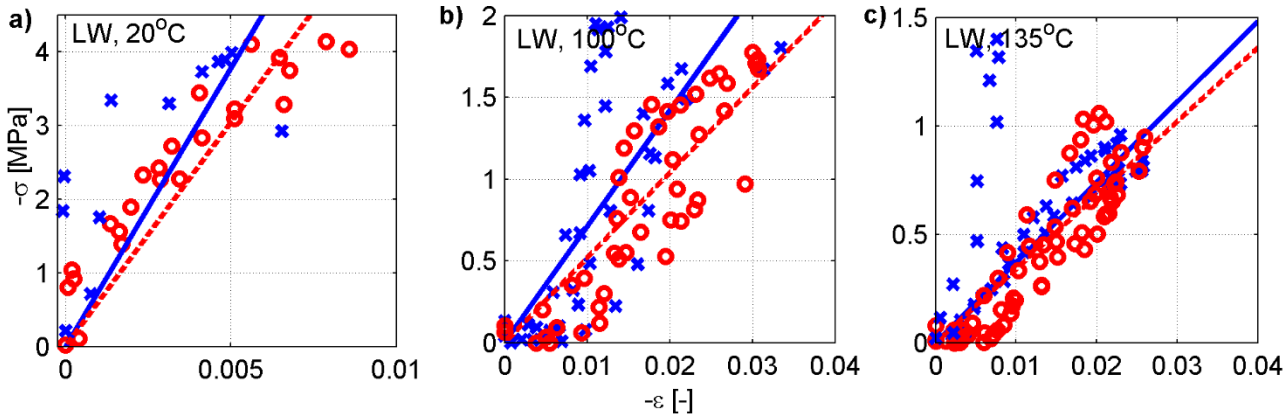

FIGURE 16 Measurement data and compression model for native (blue **x** and solid line) and fatigued (red **o** and dashed line) LW from high strain rate tests at a) 20°C, b) 100°C and c) 135°C.

In Figure 15 a, we can see that the collapse of the fatigued EW is modelled separately. This was not done at higher temperatures since the variation from the initial elastic behaviour was smaller. The material parameters from the compression model are presented in Table 1.

TABLE 1 High strain rate compression model parameters for native and fatigued wood at 20°C, 100°C and 135°C.

	ε_y^{EW} -	ε_d^{EW} -	E_e^{EW} MPa	E_p^{EW} MPa	E_d^{EW} MPa	E_e^{LW} MPa
Native 20°C	-0.009	-0.40	349	3	8	378
Fatigued 20°C	-0.008	-0.12	295	11	3	304
Native 100°C	-0.07	-	25	0.03	-	72
Fatigued 100°C	-0.41	-	4	0.7	-	52
Native 135°C	-0.05	-	16	0.4	-	37
Fatigued 135°C	-0.22	-	4	0.3	-	34

The increase in temperature softens the wood significantly. The Young's modulus for the EW was reduced by 93 % when the temperature was increased from 20°C to 100°C. The Young's modulus for the LW was probably affected by the nearby EW, since it is of the same order of magnitude. The Young's modulus for the LW was expected to be approximately double that of the EW, as demonstrated in (Farruggia & Perré 2000).

7.4 Dynamic compression model

The previously presented models (from Publication III) are referred to as the compression models, and the models presented below, which take the strain rates into account, are referred to as the dynamic models. The dynamic models were presented in Publication IV. For the dynamic material models, the parameters ε_e^{EW}, E_e^{EW}, E_p^{EW} and E_e^{LW} were fitted for the quasi-static measurement data and the parameters η^{EW} and η^{LW} were fitted to the high strain rate measurement data (with the parameters ε_e^{EW}, E_e^{EW}, E_p^{EW} and E_e^{LW} locked). The models are mainly based on four parallel samples, but only three of the fatigued samples tested at high strain rate at 100°C could be analysed. The dynamic compression models for the EW are plotted against experimental data in Figure 17, and the material parameters are presented in Table 2.

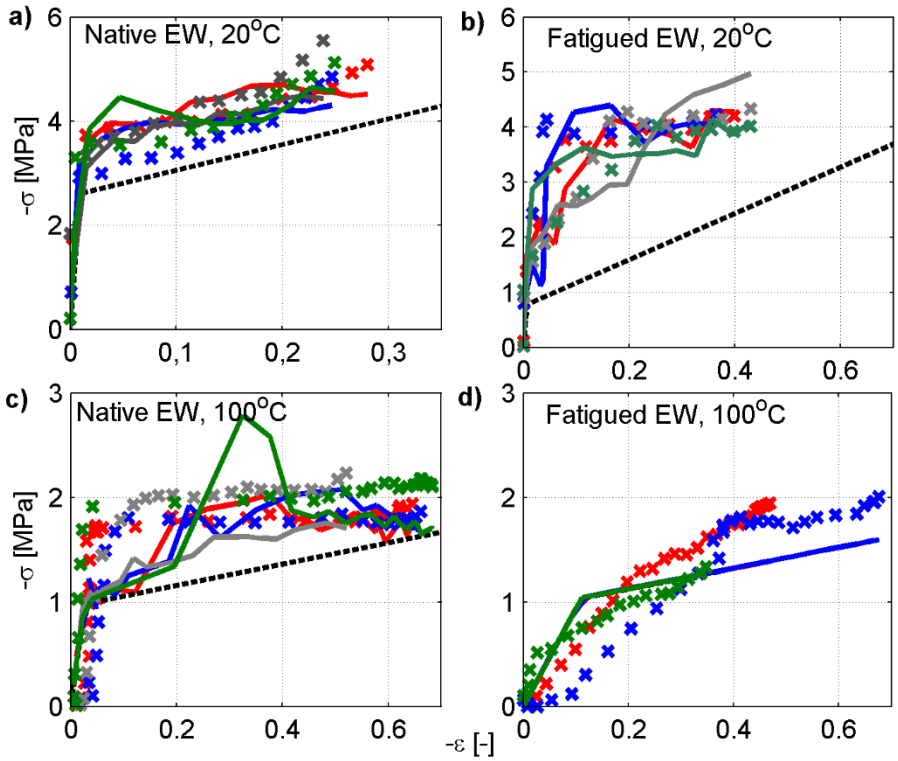

FIGURE 17 Dynamic EW material model (red, blue, green and grey solid line) and high strain rate experimental data (red **x**, blue **x**, green **x** and grey **x**) and without the term $\dot{\varepsilon}\eta$ (black dashed line) for a) native EW at 20°C, b) fatigued EW at 20°C, c) native EW at 100°C, and d) fatigued EW at 100°C.

The η^{EW} parameter for fatigued wood at 100°C is so small that the model for the different samples overlap and are the same as those for the model without the strain rate-dependent term $\dot{\varepsilon}\eta$ in Figure 17 d. The dynamic compression model for the LW is plotted with experimental data in Figure 18 and the material parameters for the LW are presented in Table 2.

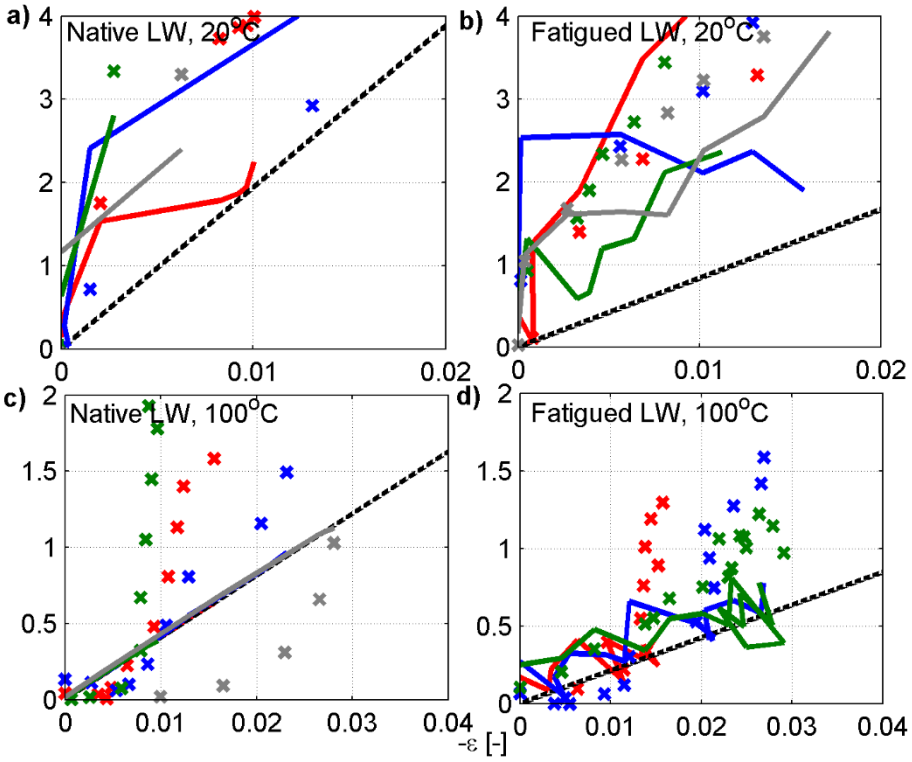

FIGURE 18 Dynamic LW material model (red, blue, green and grey solid line) and high strain rate experimental data (red **x**, blue **x**, green **x** and grey **x**) and without the term $\dot{\varepsilon}\eta$ (black dashed line) for a) native LW at 20°C, b) fatigued LW at 20°C, c) native LW at 100°C and d) fatigued LW at 100°C.

TABLE 2 Dynamic compression model parameters for native and fatigued wood at 20°C and 100°C.

	ε_y^{EW} -	E_e^{EW} MPa	E_p^{EW} MPa	η^{EW} kPa·s	E_e^{LW} MPa	η^{LW} kPa·s
Native 20°C	-0.019	133.9	2.5	0.39	194.0	1.9
Fatigued 20°C	-0.008	99.6	4.1	0.83	83.0	1.9
Native 100°C	-0.027	36.2	1.0	0.1	40.7	0.83
Fatigued 100°C	-0.112	9.3	1.0	0.0012	21.1	0.62

A quasi-static compression (i.e. without the term $\dot{\varepsilon}\eta$) of an artificial sample at 20°C was simulated with Comsol multiphysics for Publication V. The LW was modelled as a linear elastic material and the EW as an elasto-plastic material according to Eq. 9-10 and Table 2. The simulation compressed the material by 1 mm. The modelled result is presented with a measured strain distribution at the same average strain in Figure 19.

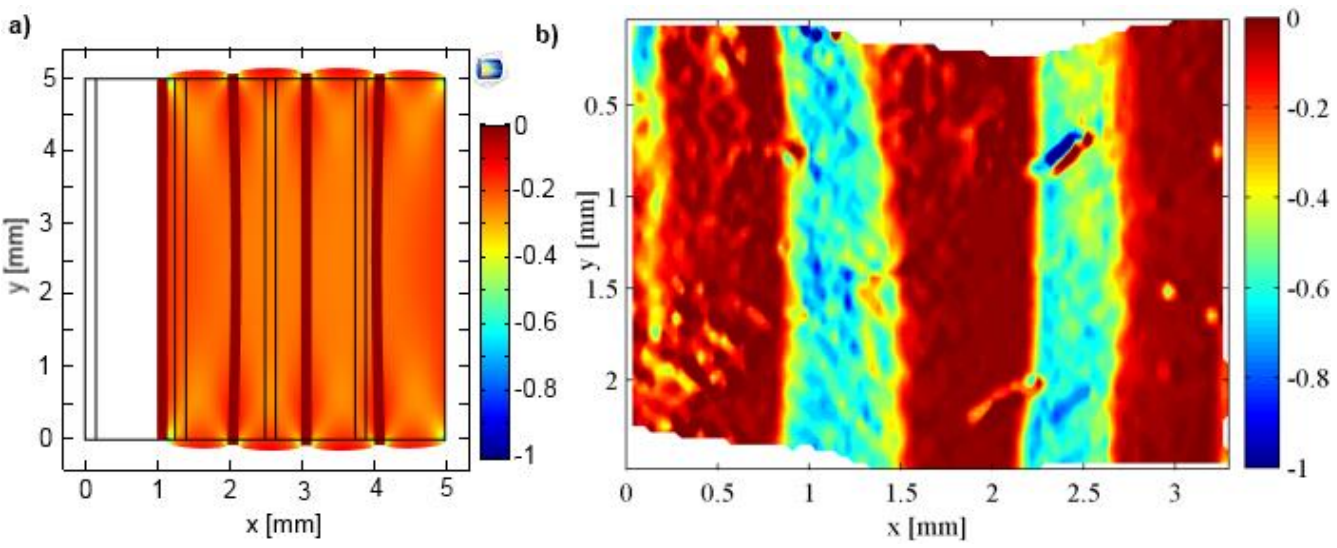

FIGURE 19 Strain distributions from a) simulation and b) quasi-static compression test.

The stress in the simulation was -3.5 MPa, while the actual measured stress was -3.4 MPa at the same average strain. The main difference between the simulation and the real measurement is that the simulated sample does not have transition wood, which makes the uncompressed part of the simulated sample significantly smaller than for the measured sample. In the measured sample, part of the transition wood has collapsed but some remains uncompressed. Since both the simulated and the measured samples are compressed to the same average strain, but the simulated sample has less uncompressed wood, the strain in the compressed part of the simulated sample must be smaller than in the measured sample.

7. Results

8 Discussion

The image-based SHPB analysis is applicable to all split-Hopkins measurements, regardless of the sample material. The method is especially valuable when traditional strain gauge measurements are hard to implement, or when full-field data is needed. The cross correlation method from PIV analysis allows the sample's texture to disappear between frames, since this gives the most probable displacement. This is especially important for wood, since the fibres collapse during compression. Both average strain and average stress calculated with the image-based method were in line with the strain gauge measurements.

The images confirm that no collapse of fibres occurs before the yield point at 20°C for native wood. The same situation was observed at a higher temperature. For fatigued wood, a slight change of slope can be seen at the marked position before the yield point in Figure 9 a. This is the point where the pre-fatigued EW fibres start to collapse. Figures 9 d and 10 d both have transition wood fibres that have not collapsed; this confirms that the densification region was not reached in the high strain rate measurements. This meant that the densification could not be modelled, so the EW model was reduced to a two-part linear model.

Of the chemical and mechanical pre-treatments included in this study, the mechanical pre-treatment reduces the elastic modulus for EW more efficiently than chemical pre-treatment at 100°C. The sulphite charge (4 %) should not be the reason for the notably small softening seen by the chemical pre-treatment, since smaller sulphite charges has shown improvements of the pulp properties (Chagaev et al. 2005; Nelsson et al. 2017). However, sulphonation does not affect the elastic modulus, but rather the plateau stress. The plateau stress was not chosen as measure of the softening in this study. Another possible reason for the small softening of the chemically pre-treated samples is that the softening due to the temperature is more significant. The effect of mechanical pre-treatment on EW is less

significant at 135°C. Chemically pre-treated samples were not tested at 135°C, since the effect was so small at 100°C that it was assumed it would be even smaller at higher temperatures. Neither mechanical nor chemical pre-treatment had any effect on LW compression.

The wood compression model is designed for applications in mechanical pulping. Therefore, the measurements are conducted on wood with an MC of 30 %. The raw material in mechanical pulping has higher MC (40-50 %), but free water would then spray out of the lumen causing problems for the image-based measurement. However, the difference does not affect the physical properties of wood significantly (Engelund et al. 2013). The E_e^{EW} for native EW at 20°C from the compression model (Table 1 and Publication III) was approximately half of that presented by Farruggia and Perré (2000). The reason for this is most likely that Farruggia and Perré worked with dry wood (MC 7 %). The E_e^{EW} for native wood at 20°C in the dynamic model is even lower. Brabec et al. (2015) and Milch et al. (2016) reported E_e values for Norway spruce (not EW) that were close to the native wood at 20°C in Table 1.

The analysis of the LW compression is probably influenced by adjacent EW for some of the samples, especially at 20°C. In both the compression model (Publication III) and the dynamic model (Publication IV), the E_e^{LW} is of the same magnitude as the E_e^{EW}, in contrast to Farruggia and Perré (2000), who reported 65 % larger values for the LW than for the EW. The values for E_e^{LW} at 100-135°C in the compression model for fatigued wood at 100°C in the dynamical model are at least double that of the E_e^{EW}.

The strain rate dependent parameters η^{EW} and η^{LW} approach zero at higher temperatures. This indicates that the wood compression is not strain rate-dependent at a high temperature. Additionally, the difference between native and fatigued wood is reduced for most material parameters (not η^{LW} and ε_y^{EW}) when the temperature is increased. This indicates that temperature is more important than pre-fatigue for wood softening.

8.1 Uncertainty

The models presented are only valid for moist wood at the specified temperatures and fatigue states. The compression model in Publication III that is presented in Table 1 is only valid at the specific strain rate used for the experiment. However, the strain rate of wood in mechanical pulping is approximately the same as in the experiments (Widehammar 2002). The conditions in mechanical pulping are compared to the experimental conditions

and the model prediction range in Table 3. Note that the strain rate (s^{-1}) is the compression rate and not the frequency of repeated compressions.

TABLE 3 Comparison of conditions in mechanical pulping to experimental work and model prediction range.

	Mechanical pulping	Experimental	Model prediction range
Strain rate [s^{-1}]	1 000 (Widehammar 2002)	0, 800-2 400	0-2 400
Temperature [°C]	100-150	20,100,135	20-100
MC [%]	40-50	30	30-50

The magnitude of noise in the image-based strain measurement was studied by analysing a reference series of images that involved no movement. The measurement noise in the strain measurement was of the order ±0.05, although some outliers were spotted at ±0.1. A typical probability density function as a function of the measurement noise was presented in Publication I. The effect of the measurement noise is further reduced in the strain calculation, since the strain is calculated as the average of four points.

The 95 % confidence intervals for the dynamic model presented in Publication IV are presented in Table 4. It is assumed that the confidence intervals would be of similar magnitude for the compression model presented in Publication III. The primary use of the compression model is also for comparison of the parameters of different fatigue stages and temperatures, as well as for comparison with the work of other researchers. Further validation of the dynamic model is given by the comparison of measured and simulated strain in Figure 19.

TABLE 4 The confidence intervals for the dynamic compression model material parameters.

	ε_y^{EW}	E_e^{EW} MPa	E_p^{EW} MPa	η^{EW} kPa·s	E_e^{LW} MPa	η^{LW} kPa·s
Native 20°C	-0.021 – -0.018	124.6-143.3	2.2-2.7	0.33-0.46	181.6-206.4	1.6-2.2
Fatigued 20°C	-0.012 – -0.004	53.9-145.3	3.4-4.8	0.74-0.92	72.7-93.4	1.7-2.0
Native 100°C	-0.032 – -0.023	30.3-42.1	0.9-1.1	0.074-0.13	34.2-47.2	0.54-1.1
Fatigued 100°C	-0.116 – -0.107	9.0-9.6	0.9-1.1	-0.032-0.035	19.7-22.6	0.50-0.75

8.2 Conclusions

The hypothesis that was presented in the introduction was correct: image based analysis and modelling is well suited for studying the difference in compression behaviour of earlywood and latewood according to the initial simulation results. The local compression behaviour is important for the mechanical pulping process. The presented wood models are the first wood compression models for high strain rate and high temperature compression of moist wood that are divided into EW and LW. The conclusions of this thesis are best presented by returning to the research questions asked in the introduction:

Q1. What kind of compression models already exist, and how can a compression model for wood be developed that can adequately describe the behaviour of wood under rapid compression?

The most important result of this thesis is the dynamic wood compression model. Alternative material models were discussed in detail in Chapter 5. The proposed wood compression model for optimization of the mechanical pulping process is a simple Voigt-Kelvin model that is defined in parts for EW and a simple Voigt-Kelvin model for the LW. This is simple enough for researchers who are not specialized in material modelling to be able to understand and use the model in modern simulation software.

Q2. What kind of experimental data is needed to develop a material model for wood compression and how can the required experimental results be achieved?

The material model needs to be based on full-field quasi-static and high strain rate experimental data at room temperature and at high temperatures. The full-field data needs to be reduced to EW and LW compression. For this, a new image-based analysis method for the SHPB was developed. The method is especially valuable for analysis of

soft, heterogeneous materials. High strain rate and quasi-static compression data of Norway spruce EW and LW were collected at 20°C and 80-100°C. High strain rate compression data was also collected at 135°C.

8.3 Implications for mechanical pulping

Energy efficient internal and external defibration is the final goal in mechanical pulping. Wood compression modelling on the level of strain and stress does not directly reveal level of internal and external defibration. However, the strain and stress development can be used to estimate these levels. E.g., a drop in elasticity modulus can be connected to internal fibre defibration and fibre surface stress caused by defibration tool can be connected to external fibre defibration.

The fibre needs to be flexible in all directions for good paper quality. The advancing cyclic compression experiment showed clearly that identically repeating strain does not increase fatigue, either as new collapse patterns on fibre level or as lowered elastic modulus. The fibre should be compressed in different directions in order to achieve the desired flexibility in all directions. The same experiment also indicates that enough large single compression strain pulses should be offered by defibration tools to reach high efficiency in internal fibrillation. Uhmeier and Salmén (1996b) suggested that a small number of large compressions could be an energy efficient way to increase the collapsibility of the fibres and we can see that the repeated loading does not significantly soften the fibres.

The wood softens significantly with increased temperature. We could see that the maximum strain achieved increased with increasing temperature and that the maximum stress achieved decreased. Salmén and Fellers (1982) found that the separation take place in the middle lamella at 100°C and along the cell wall at 80°C. For paper production, it is important that fibres are separated at along the cell wall and not at the middle lamella, Salmén and Fellers therefore suggested that the defibration and fibre development are carried out at different temperatures.

The research presented in this thesis shows the different compression behaviour of EW and LW. The LW was not significantly compressed in the experiments. This suggests that the EW and LW fibres needs different kinds of loading to be developed efficiently. This was also suggested by Salmén et al (1997). The mechanical pulping processes takes this partly into account automatically when the flexible fibres can deflect and the stiffer fibres takes the load.

The novelty value of this thesis is however the wood compression model, that allows modelling of wood response to different compressions. This tool can be used for the development of new grinding surfaces and refiner plates.

8.4 Future work

The most important recommendation for future work is to use the dynamic compression model. So far, only initial quasi-static simulations have been done for verification purposes. Simulations, which validate the main purpose of the model, i.e. to make improvements to the mechanical pulping process, have not been done. However, the presented dynamic compression model is suitable for such simulations.

For improved accuracy, the wood model could be extended to also take the transition wood into account. This can be done based on the experimental data gathered for this thesis. Improvements to the model that would require further experimental work include more measurements at additional temperatures and additional fatigue stages in order to present the material parameters as functions of temperature and the state of fatigue. The tangential and radial directions could also be added to the model.

References

Abe, H., Ohtani, J. & Fukazawa, K. (1991). Fe-Sem Observations on the Microfibrillar Orientation in the Secondary Wall of Tracheids, IAWA Journal, Vol. 12(4), pp. 431-438.

Adalian, C. & Morlier, P. (2001). A model for the behaviour of wood under dynamic multiaxial compression, Composites Science and Technology, Vol. 61(3), pp. 403-408.

Ando, K. & Onda, H. (1999). Mechanism for deformation of wood as a honeycomb structure II: First buckling mechanism of cell walls under radial compression using the generalized cell model, Journal of Wood Science, Vol. 45(3), pp. 250-253.

Atack, D. & Heitner, C. (1979). Dynamic mechanical properties of sulphonated eastern black spruce, Transactions of the Technical Section - Canadian Pulp and Paper Association, Vol. 5(4), pp. 99-108.

Bergander, A. & Salmen, L. (2000). Transverse elastic modulus of the native wood fibre wall, Journal of Pulp and Paper Science, Vol. 26(6), pp. 234-238.

Björkqvist, T. (2002). A design method for an efficient fatigue process in wood grinding - an analytical approach, Doctoral Thesis, Tampere University of Technology, Tampere, Finland, 104 p.

Björkqvist, T., Lautala, P., Saharinen, E., Paulapuro, H., Koskenhely, K. & Lönnberg, B. (1999). Behaviour of spruce sapwood in mechanical loading, Journal of Pulp and Paper Science, Vol. 25(4), pp. 118-123.

Boutelje, J.B. (1962). The Relationship of Structure to Transverse Anisotropy in Wood with Reference to Shrinkage and Elasticity, Holzforschung, Vol. 16(2), pp. 33-46.

Brabec, M., Tippner, J., Sebera, V., Milch, J. & Rademacher, P. (2015). Standard and non-standard deformation behaviour of European beech and Norway spruce during compression, Holzforschung, Vol. 69(9), pp. 1107-1116.

Bragov, A. & Lomunov, A.K. (1997). Dynamic properties of some wood species, Journal De Physique.IV : JP, Vol. 7(3), pp. 487-492.

References

Bruck, H.A., McNeill, S.R., Sutton, M.A. & Peters, W.H. (1989). Digital image correlation using Newton-Raphson method of partial differential correction, Experimental Mechanics, Vol. 29(3), pp. 261-267.

Cave, I.D. (1976). Modelling the structure of the softwood cell wall for computation of mechanical properties, Wood Science and Technology, Vol. 10(1), pp. 19-28.

Chagaev, O., Heitner, C. & Hellstern, M. (2005). The effects of sulphonation and high-intensity refining on the ultra-high-yield pulping of spruce, Pulp and Paper Canada, Vol. 106(12), pp. 65-70.

Choi, D., Thorpe, J.L. & Hanna, R.B. (1991). Image analysis to measure strain in wood and paper, Wood Science and Technology, Vol. 25(4), pp. 251-262.

Cramer, S., Kretschmann, D., Lakes, R. & Schmidt, T. (2005). Earlywood and latewood elastic properties in loblolly pine, Holzforschung, Vol. 59(5), pp. 531-538.

Dahl, K.B. & Malo, K.A. (2009). Planar strain measurements on wood specimens, Experimental Mechanics, Vol. 49(4), pp. 575-586.

Davies, R.M. (1948). A critical study of the Hopkinson pressure bar, Philos. Trans. R. Soc. London, Sect. B, Vol. 240(821), pp. 375-457.

Davies, E.D.H. & Hunter, S.C. (1963). The dynamic compression testing of solids by the method of the split Hopkinson pressure bar, Journal of the Mechanics and Physics of Solids, Vol. 11(3), pp. 155-179.

De Magistris, F. (2005). Wood fibre deformation in combined shear and compression, Doctoral Thesis, KTH Royal Institute of Technology, Stockholm Sweden, 49 p.

Dumail, J.F. & Salmén, L. (1996). Compression behaviour of spruce wood under large plastic deformations, Nordic Pulp and Paper Research Journal, Vol. 11(4), pp. 239-242.

Eder, M., Jungnikl, K. & Burgert, I. (2009). A close-up view of wood structure and properties across a growth ring of Norway spruce (Picea abies [L] Karst.), Trees - Structure and Function, Vol. 23(1), pp. 79-84.

Engberg, B.A., Logenius, L. & Engstrand, P. (2014). Mechanical properties of sulphonated wood in relation to wing refiner pulp properties, Proceedings of the International mechanical pulping conference, June 2-5, Helsinki, Finland.

Engelund, E.T., Thygesen, L.G., Svensson, S. & Hill, C.A.S. (2013). A critical discussion of the physics of wood-water interactions, Wood Science and Technology, Vol. 47(1), pp. 141-161.

Farruggia, F. & Perré, P. (2000). Microscopic tensile tests in the transverse plane of earlywood and latewood parts of spruce, Wood Science and Technology, Vol. 34(2), pp. 65-82.

Fortino, S., Hradil, P., Salminen, L. & De Magistris, F. (2015). A 3D micromechanical study of deformation curves and cell wall stresses in wood under transverse loading, Journal of Materials Science, Vol. 50(1), pp. 482-492.

Gama, B.A. (2004). Hopkinson bar experimental technique: A critical review, Applied Mechanics Reviews, Vol. 57(4), pp. 223-250.

Gibson, L.J. & Ashby, M.F. (1997). Cellular solids structure and properties, Second edition ed., Cambridge University Press, Cambridge, United Kingdom, 510 p.

Gilat, A., Schmidt, T. & Walker, A. (2009). Full Field Strain Measurement in Compression and tensile Split Hopkinson Bar Experiments, Exp.Mech., Vol. 49pp. 291-302.

Grantham, S.G., Siviour, C.R., Proud, W.G. & Field, J.E. (2004). High-strain rate Brazilian testing of an explosive simulant using speckle metrology, Meas. Sci. Technol, Vol. 15pp. 1867-1870.

Gray III, G.T. (2000). Classic Split-Hopkinson Pressure Bar Testing, in: Vol 8 Mechanical Testing and Evaluation, ASM Handbook, ASM International, pp. 462-476.

Gray III, G.T. & Blumenthal, W.R. (2000). Split-Hopkinson Pressure Bar Testing of Soft Materials, in: *Mechanical Testing and Evaluation*, Vol 8, *ASM Handbook*, ASM International, pp. 488-496.

Grédiac, M. & Hild, F. (2013). Full-Field Measurements and Identification in Solid Mechanics, Wiley, London, United Kingdom, 476 p.

Guitard, D., Masse, H., Yamamoto, H. & Okuyama, T. (1999). Growth stress generation: A new mechanical model of the dimensional change of wood cells during maturation, Journal of Wood Science, Vol. 45(5), pp. 384-391.

Hamad, W.Y. & Provan, J.W. (1995). Microstructural cumulative material degradation and fatigue-failure micromechanisms in wood-pulp fibres, Cellulose, Vol. 2(3), pp. 159-177.

Hanhijärvi A. & Mackenzie-Helnwein P. (2003). Computational analysis of quality reduction during drying of lumber due to irrecoverable deformation. I: Orthotropic viscoelastic-mechanosorptive-plastic material model for the transverse plane of wood, Journal of Engineering Mechanics, Vol. 129(9), pp. 996-1005.

Hassel, B.I., Modén, C.S. & Berglund, L.A. (2009). Functional gradient effects explain the low transverse shear modulus in spruce - Full-field strain data and a micromechanics model, Composites Science and Technology, Vol. 69(14), pp. 2491-2496.

Heitner, C. & Salmén, L. (1994). The effect of sulphonation on the fatigue properties of wood, Nordic Pulp and Paper Research Journal, Vol. 9(3), pp. 182-186.

Hickey, K.L. & Rudie, A.W. (1993). Preferential Energy absorption by Earlywood in cyclic compression of Loblolly pine, International Mechanical Pulping Conference, June 15-17, Oslo, Norway, pp. 81-86.

Hofstetter, K., Hellmich, C. & Eberhardsteiner, J. (2005). Development and experimental validation of a continuum micromechanics model for the elasticity of wood, European Journal of Mechanics, A/Solids, Vol. 24(6), pp. 1030-1053.

Holmberg, S. (1998). A numerical and experimental study of initial defibration of wood, Doctoral Thesis, Lund University, Structural Mechanics, Lund, Sweden, 203 p.

References

Holmgren, S., Svensson, B.A., Gradin, P.A. & Lundberg, B. (2008). An encapsulated split Hopkinson pressure bar for testing of wood at elevated strain rate, temperature, and pressure, Experimental Techniques, Vol. 32(5), pp. 44-50.

Hopkinson, B. (1914). A Method of Measuring the Pressure in the Detonation of High Explosives or by the Impact of Bullets, Philos. Trans. R. Soc. London, Ser. A, Vol. 213, pp. 437-456.

Huang, F., Lanouette, R. & Law, K.N. (2007). Jack pine tmp: Earlywood versus latewood and effect of refining temperature, International Mechanical Pulping Conference 2007, TAPPI, pp. 418-451.

Isaksson, P., Gradin, P.A. & Hellström, L.M. (2013). A numerical and experimental study regarding the influence of some process parameters on the damage state in wood chips, Holzforschung, Vol. 67(6), pp. 691-696.

Jernkvist, L.O. & Thuvander, F. (2001). Experimental determination of stiffness variation across growth rings in Picea abies, Holzforschung, Vol. 55(3), pp. 309-317.

Karlström, A. & Eriksson, K. (2014). Fiber energy efficiency Part IV: Multi-scale modeling of refining processes, Nordic Pulp and Paper Research Journal, Vol. 29(3), pp. 409-417.

Kollman, F.F. & Côte, W.A. (1968). Principles of Wood Science and Technology, Volume 1 Solid Wood. Vol. 1 ed., Springer-Verlag, New York, USA, 592 p.

Kolsky, H. (1949). An investigation of the mechanical properties of materials at very high rates of loading, Proc. Phys. Soc. London, Sect. B, Vol. 62(II-B), pp. 676-700.

Koponen, S., Toratti, T. & Kanerva, P. (1991). Modelling elastic and shrinkage properties of wood based on cell structure, Wood Science and Technology, Vol. 25(1), pp. 25-32.

Koponen, S., Toratti, T. & Kanerva, P. (1989). Modelling longitudinal elastic and shrinkage properties of wood, Wood Science and Technology, Vol. 23(1), pp. 55-63.

Kure, K.A., Dahlqvist, D., Sabourin, M.J. & Helle, T. (1999). Development of spruce fiber properties by a combination of a pressurized compressive pretreatment and high intensity refining, International Mechanical Pulping Conference, May 24-26, TAPPI, Houston, USA, pp. 427-433.

Law, K.N., Kokta, B.V. & Mao, C. (2006). Compression properties of wood and fibre failures, Journal of Pulp and Paper Science, Vol. 32(4), pp. 224-230.

Lee, S., Hwang, J., Ravi Shankar, M., Chandrasekar, S. & Compton, W.D. (2006). Large strain deformation field in machining, Metallurgical and Materials Transactions A: Physical Metallurgy and Materials Science, Vol. 37(5), pp. 1633-1643.

Logenius, L., Engberg, B.A., Nelsson, E. & Engstrand, P. (2013). Mechanical testing methods for evaluation of the mechanical properties of sulphonated wood, The 17th International Symposium on Wood, Fiber and Pulping Chemistry, 12-14 June 2013, Vancouver, Canada.

Lucander, M., Asikainen, S., Pöhler, T., Saharinen, E. & Björkqvist, T. (2009). Fatigue treatment of wood by high-frequency cyclic loading, Journal of Pulp and Paper Science, Vol. 35(3-4), pp. 81-85.

Mao, C., Law, K.N. & Kokta, B.V. (2004). Effect of sulfonation on the compression behaviour of early - And latewood, Pulp and Paper Canada, Vol. 105(12), pp. 67-71.

Mauranen, A., Ovaska, M., Koivisto, J., Salminen, L.I. & Alava, M. (2015). Thermal conductivity of wood: effect of fatigue treatment, Wood Science and Technology, Vol. 49(2), pp. 359-370.

Miksic, A., Myntti, M., Koivisto, J., Salminen, L. & Alava, M. (2013). Effect of fatigue and annual rings orientation on mechanical properties of wood under cross-grain uniaxial compression, Wood Science and Technology, Vol. 47(6), pp. 1117-1133.

Milch, J., Tippner, J., Sebera, V. & Brabec, M. (2016). Determination of the elasto-plastic material characteristics of Norway spruce and European beech wood by experimental and numerical analyses, Holzforschung, Vol. 70(11), pp. 1081-1092.

Mishnaevsky Jr., L. & Qing, H. (2008). Micromechanical modelling of mechanical behaviour and strength of wood: State-of-the-art review, Computational Materials Science, Vol. 44(2), pp. 363-370.

Moden, C.S. (2008). A two-phase annual ring model of transverse anisotropy in softwoods, Composites Science and Technology, Vol. 68(14), pp. 3020-3026.

Mohr, D., Gary, G. & Lundberg, B. (2010). Evaluation of stress-strain curve estimates in dynamic experiments, International Journal of Impact Engineering, Vol. 37(2), pp. 161-169.

Moilanen, C.S., Björkqvist, T. & Saarenrinne, P. (2015). Wood compression model for radial compression of earlywood and latewood, Proceedings of the XII Finnish Mechanics Days, June 4th-5th 2015, Tampere, Finland, pp. 261-266.

Moilanen, C.S., Saarenrinne, P., Engberg, B.A. & Björkqvist, T. (2014). Image Based Local Strain Measurement of Wood, in: Jin, H., Sciammarella, C., Yoshida, S. & Lamberti, L. (ed.), Advancement of Optical Methods in Experimental Mechanics, Volume 3, SEM Annual conference, Lombard IL, June 3rd-5th 2013 ed., Springer International Publishing, pp. 339-345.

Murton, K.D., Richardson, J.D., Corson, S.R. & Duffy, G.G. (2001). TMP refining of radiata pine earlywood and latewood fibres, International Mechanical Pulping Conference, June 4-8, Helsinki, Finland, pp. 361-371.

Müller, U., Gindl, W. & Teischinger, A. (2003). Effects of cell anatomy on the plastic and elastic behaviour of different wood species loaded perpendicular to grain, IAWA Journal, Vol. 24(2), pp. 117-128.

Nelsson, E., Paulsson, M., Sandberg, C., Svensson-Rundlöf, E. & Engstrand, P. (2017). Low dosage sulfite pretreatment at different refining temperatures in mill scale TMP production, Nordic Pulp and Paper Research Journal, Vol. 32(1), 59-69.

Oscarsson, J., Olsson, A. & Enquist, B. (2012). Strain fields around knots in Norway spruce specimens exposed to tensile forces, Wood Science and Technology, Vol. 46(4), pp. 593-610.

Pan, B., Qian, K., Xie, H. & Asundi, A. (2009a). Two-dimensional digital image correlation for in-plane displacement and strain measurement: A review, Measurement Science and Technology, Vol. 20(6), pp. 062001.

Pan, B., Asundi, A., Xie, H. & Gao, J. (2009b). Digital image correlation using iterative least squares and pointwise least squares for displacement field and strain field measurements, Optics and Lasers in Engineering, Vol. 47(7–8), pp. 865-874.

Persson, K. (2000). Micromechanical modelling of wood and fibre properties, Doctoral Thesis, Lund University, Lund, Sweden, 213 p.

Petzing, J.N. & Tyrer, J.R. (1998). Recent developments and applications in electronic speckle pattern interferometry, The Journal of Strain Analysis for, Vol. 33(2), pp. 153-169.

Raffel, M., Willert, C.E., Wereley, S.T. & Kompenhans, J. (2007). Particle Image Velocimetry, A Practical Guide, Second Edition ed., Springer-Verlag, Berlin Heidelberg, Germany, 448 p.

Reid, S.R. & Peng, C. (1997). Dynamic uniaxial crushing of wood, International Journal of Impact Engineering, Vol. 19(5-6), pp. 531-570.

Renaud, M., Rueff, M. & Rocaboy, A.C. (1996b). Mechanical behaviour of saturated wood under compression Part 2: Behaviour of wood at low rates of strain some effects of compression on wood structure, Wood Science and Technology, Vol. 30(4), pp. 237-243.

Renaud, M., Rueff, M. & Rocaboy, A.C. (1996a). Mechanical behaviour of saturated wood under compression: Part 1. Behaviour of wood at high rates of strain, Wood Science and Technology, Vol. 30(3), pp. 153-164.

Saari, V., Björkqvist, T., Engberg, B.A. & Saarenrinne, P. (2009). Strain distribution in annual rings under compression by high speed photography, International Mechanical Pulping Conference, 31 May - 4 June, Sundsvall, Sweden.

Saavedra Flores, E.I., De Souza Neto, E.A. & Pearce, C. (2011). A large strain computational multi-scale model for the dissipative behaviour of wood cell-wall, Computational Materials Science, Vol. 50(3), pp. 1202-1211.

Salmen, L. (1987). The Effect of the Frequency of a Mechanical Deformation on the Fatigue of Wood, Journal of Pulp and Paper Science, Vol. 13(1), pp. 23-28.

Salmen, L., Tigerstrom, A. & Fellers, C. (1985). Fatigue of Wood - Characterization of Mechanical Defibration, Journal of Pulp and Paper Science, Vol. 11(3), pp. 68-73.

Salmen, N.L. & Fellers, C. (1982). The Fundamentals of Energy Consumption during Viscoelastic and Plastic Deformation of Wood , Transactions of the Technical Section - Canadian Pulp and Paper Association, Vol. 8(4), pp. tr93-tr99.

Salmi, A., Saharinen, E. & Hæggström, E. (2011). Layer-like fatigue is induced during mechanical pulping, Cellulose, Vol. 18(6), pp. 1423-1432.

Salmi, A., Salminen, L.I., Engberg, B.A., Björkqvist, T. & Hæggström, E. (2012a). Repetitive impact loading causes local plastic deformation in wood, Journal of Applied Physics, Vol. 111(2), pp. 024901.

Salmi, A., Salminen, L.I., Lucander, M. & Hæggström, E. (2012b). Significance of fatigue for mechanical defibration, Cellulose, Vol. 19(2), pp. 575-579.

Salmi, A., Salminen, L. & Hæggström, E. (2009). Quantifying fatigue generated in high strain rate cyclic loading of Norway spruce, Journal of Applied Physics, Vol. 106(10), pp. 104905.

Salmén, L., Dumail, J.F. & Uhmeier, A. (1997). Compression behaviour of wood in relation to mechanical pulping, Proceedings of the International Mechanical Pulping Conference, June 9-13, Stockholm, pp. 207-211.

Serrano, E. & Enquist, B. (2005). Contact-free measurement and non-linear finite element analyses of strain distribution along wood adhesive bonds, Holzforschung, Vol. 59(6), pp. 641-646.

Siviour, C.R. (2009). A measurement of wave propagation in the split Hopkinson pressure bar, Measurement Science and Technology, Vol. 20(6), pp. 065702.

Sutton, M., Orteau, J.J. & Schreier, H. (2009). Image Correlation for Shape, Motion and Deformation Measurements, Springer, New York, USA, 321 p.

Tabarsa, T. & Chui, Y.H. (2001). Characterizing microscopic behavior of wood under transverse compression. Part II. Effect of species and loading direction, Wood and Fiber Science, Vol. 33(2), pp. 223-232.

Thuvander, F., Sjödahl, M. & Berglund, L.A. (2000). Measurements of crack tip strain field in wood at the scale of growth rings, Journal of Materials Science, Vol. 35(24), pp. 6267-6275.

Uhmeier, A., Morooka, T. & Norimoto, M. (1998). Influence of thermal softening and degradation on the radial compression behavior of wet spruce, Holzforschung, Vol. 52(1), pp. 77-81.

Uhmeier, A. & Salmén, L. (1996a). Influence of strain rate and temperature on the radial compression behavior of wet spruce, Journal of Engineering Materials and Technology, Transactions of the ASME, Vol. 118(3), pp. 289-294.

Uhmeier, A. & Salmén, L. (1996b). Repeated large radial compression of heated spruce, Nordic Pulp and Paper Research Journal, Vol. 11(3), pp. 171-176.

Valla, A., Konnerth, D., Keunecke, D., Niemz, P., Muller, U. & Gindl, W. (2011). Comparison of two optical methods for contactless, full field and highly sensitive in-plane deformation measurements using the example of plywood, Wood Sci.Technol., Vol. 45, pp. 755-765.

Vessby, J., Serrano, E. & Enquist, B. (2010). Contact-free measurement and numerical and analytical evaluation of the strain distribution in a wood-FRP lap-joint, Mater.Struct., Vol. 43, pp. 1085-1095.

Viforr, S. & Salmén, L. (2008). Shear/compression of chips for lower energy consumption in TMP refining, Appita Journal, Vol. 61(1), pp. 49-55.

Watanabe, U., Fujita, M. & Norimoto, M. (2002). Transverse Young's moduli and cell shapes in coniferous early wood, Holzforschung, Vol. 56(1), pp. 1-6.

Wennerblom, M., Olsson, A.-. & Salmén, L. (1996). Softening properties of early wood and latewood of spruce, Nordic Pulp and Paper Research Journal, Vol. 11(4), pp. 279-280.

Westermark, U., Samuelsson, B., Simonsson, R. & Phil, R. (1987). Investigation of a selective sulfonation of wood chips Part 5. Thermomechanical pulping with low addition of sulfite, Nordic Pulp and Paper Research Journal, Vol. 2(4), pp. 146-151.

White, D.J., Take, W.A. & Bolton, M.D. (2003). Soil deformation measurement using particle image velocimetry (PIV) and photogrammetry, Geotechnique, Vol. 53(7), pp. 619-631.

Widehammar, S. (2002). A Method for Dispersive Split Hopkinson Pressure Bar Analysis Applied to High Strain Rate Testing of Spruce Wood, Doctoral Thesis, Uppsala University, Uppsala Sweden, 41 p.

Widehammar, S. (2004). Stress-strain relationships for spruce wood: Influence of strain rate, moisture content and loading direction, Experimental Mechanics, Vol. 44(1), pp. 44-48.

Wykes, C. (1982). Use of electronic speckle pattern interferometry (ESPI) in the measurement of static and dynamic surface displacements. Optical Engineering, Vol. 21(3), pp. 400-406.

Xavier, J., Avril, S., Pierron, F. & Morais, J. (2009). Variation of transverse and shear stiffness properties of wood in a tree, Composites Part A: Applied Science and Manufacturing, Vol. 40(12), pp. 1953-1960.

Yamamoto, H. (1998). Generation mechanism of growth stresses in wood cell walls: Roles of lignin deposition and cellulose microfibril during cell wall maturation, Wood Science and Technology, Vol. 32(3), pp. 171-182.

Yang, L.M. (2005). An analysis of stress uniformity in split Hopkinson bar test specimens, International Journal of Impact Engineering, Vol. 31(2), pp. 129-150.

Zink, A., Davidson, R. & Hanna, R. (1995). Strain measurement in wood using a digital image correlation technique, Wood and Fibre Science, Vol. 27, pp. 346-359.

Östberg, G. & Salmén, L. (1988). Effects of sulphonation on properties of different cell wall layers, Nordic Pulp and Paper Research Journal, Vol. 3(1), pp. 8-12.

Tampereen teknillinen yliopisto
PL 527
33101 Tampere

Tampere University of Technology
P.O.B. 527
FI-33101 Tampere, Finland

ISBN 978-952-15-4032-5
ISSN 1459-2045